Supporting Information for

Unlocking the Potential of Organopalladium Complexes for High-Grade Serous Ovarian Cancer Therapy

Thomas Scattolin,*[,a] Enrico Cavarzerani,[b] Dario Alessi,[a] Matteo Mauceri,[a] Eleonora Botter,[b] Giovanni Tonon,[b] Isabella Caligiuri,[c] Ombretta Repetto,[d] Urska Kamensek,[e] Simona Kranjc Brezar,[e] Maria Dalla Pozza,[f] Stefano Palazzolo,[c] Maja Cemazar,[e] Vincenzo Canzonieri,[c,g] Nicola Demitri,[h] Steven P. Nolan,[i] Gilles Gasser,[f] Fabiano Visentin*[b] and Flavio Rizzolio*[b,c]

[a.] *Dipartimento di Scienze Chimiche, Università degli Studi di Padova, via Marzolo 1, 35131 Padova (Italy). E-mail: thomas.scattolin@unipd.it*
[b.] *Dipartimento di Scienze Molecolari e Nanosistemi, Università Ca' Foscari, Campus Scientifico Via Torino 155, 30174 Venezia-Mestre (Italy). E-mail: fvise@unive.it and flavio.rizzolio@unive.it*
[c.] *Pathology Unit, Centro di Riferimento Oncologico di Aviano (C.R.O.) IRCCS, via Franco Gallini 2, 33081, Aviano, Italy.*
[d.] *Immunopathology and Cancer Biomarkers, Centro di Riferimento Oncologico di Aviano (CRO), IRCCS, via Franco Gallini 2, 33081, Aviano, Italy.*
[e.] *Department of Experimental Oncology, Institute of Oncology Ljubljana, Ljubljana, 1000, Slovenia.*
[f.] *ChimieParisTech, PSL University, CNRS, Institute of Chemistry for Life and Health Sciences, Laboratory for Inorganic Chemical Biology, 75005, Paris, France.*
[g.] *Department of Medical, Surgical and Health Sciences, Università degli Studi di Trieste, Strada di Fiume 447, Trieste, Italy.*
[h.] *Area Science Park, Elettra-Sincrotrone Trieste, S.S. 14 Km 163.5, Basovizza, 34149, Trieste, Italy*
[i.] *Department of Chemistry and Centre for Sustainable Chemistry, Ghent University, Krijgslaan 281, S-3, 9000 Ghent, Belgium*

Table of Contents

Experimental Section

Materials and methods

All syntheses of Pd(II)-vinyl and butadienyl complexes were carried out under an atmosphere of argon. Solvents were dried according to standard procedures. Palladium precursors **1a-b**,[1] silver NHC complexes **6**[2] and **11**,[3] and palladium complexes **5a-b**[1] were synthesized according to previously published procedures.

All other monodentate/bidentate ligands and [(PhC≡C)Sn(*n*-Bu)$_3$ were purchased from Sigma Aldrich and used without any further purification. ^{1}H, ^{13}C{^{1}H} and ^{31}P{^{1}H} NMR spectra were recorded on a Bruker Advance 400 spectrometer at room temperature (298K). The IR spectra were recorded on a Perkin-Elmer Spectrum One spectrophotometer and elemental analysis was carried out using an Elemental CHN "CUBO Micro Vario" analyzer.

ESI-MS analyses were performed using a LCQ-Duo (Thermo-Finnigan) operating in positive ion mode (capillary voltage 10 V, spray voltage 4.5 kV, capillary temperature 200 °C, mass scan range from 150 to 2000 amu). X-ray intensity data were collected at 100 K at the XRD2 beamline of the Elettra Synchrotron, Trieste (Italy).

Synthesis of [Pd(1,10-phen)Cl(C_2(COOMe)$_2$$CH_3$)] (2a)

0.0820 g (0.1594 mmol) of the palladium precursor [Pd(Me-PyCH$_2$SPh)Cl(C_2(COOMe)$_2$$CH_3$)] (**1a**) was dissolved in 15 mL of anhydrous dichloromethane in a 100 mL two-necked flask under inert atmosphere (Ar). Subsequently, 0.0316 g (0.1754 mmol) of 1,10-phenanthroline previously dissolved in ca. 5 mL of CH_2Cl_2 was added. The mixture was stirred at room temperature for 30 min and the solvent was then reduced under vacuum. The final product (pink microcrystalline powder) was precipitated by addition of diethylether and filtered off on a gooch filter.

0.0753 g of **2a** was obtained (yield 98%).

^{1}H-NMR (300 MHz, $CDCl_3$, T = 298 K, ppm) δ: 2.56 (s, 3H, =CCH_3), 3.76 (s, 3H, OCH_3), 3.86 (s, 3H, OCH_3), 7.85-7.93 (m, 2H, phen-H^3, phen-H^8), 8.00-8.02 (AB system, J = 8.9 Hz, 2H, phen-H^5, phen-H^6), 8.53-8.58 (m, 2H, phen-H^4, phen-H^7), 9.31 (dd, J = 5.2, 1.4 Hz, phen-H^9), 9.48 (dd, J = 5.0, 1.5 Hz, phen-H^2).

^{13}C{^{1}H}-NMR (T = 298K, $CDCl_3$, ppm) δ: 21.5 (CH_3, =CCH_3), 51.7 (CH_3, OCH_3), 51.9 (CH_3, OCH_3), 125.3, 125.7 (CH, phen-CH^3, phen-CH^8), 127.0, 127.2 (CH, phen-CH^5, phen-CH^6), 127.3 (C, =CCH_3), 129.6, 130.1 (C, phen-C^{13}, phen-C^{14}), 138.1, 138.2 (CH, phen-CH^4, phen-CH^7), 145.3, 147.1 (C, phen-C^{11}, phen-CH^{12}), 149.6 (CH, phen-CH^9), 153.3 (CH, phen-CH^2), 159.2 (C, Pd-C=), 163.6 (C, CO), 173.7 (C, CO).

IR (KBr pellet): $\nu_{C=O}$ = 1693 cm^{-1}

Elemental analysis calcd (%) for $C_{19}H_{17}ClN_2O_4Pd$: C, 47.62, H, 3.58, N, 5.85; found: C, 47.94, H, 3.40, N, 5.73.

Synthesis of [Pd(1,10-phen)Cl(C_4(COOMe)$_4$$CH_3$)] (2b)

Complex **2b** was prepared using a similar procedure, starting from 0.0820 g (0.1249 mmol) of the precursor [Pd(Me-PyCH_2SPh)Cl(C_4(COOMe)$_4$$CH_3$)] (**1b**) and 0.0584 g (0.1374 mmol) of 1,10-phenanthroline.
0.0692 g (yield 89%) of **2b** was obtained (pink microcrystalline powder). *n*-Hexane/diethylether (1:1) was used instead of diethylether for the precipitation of the title complex.

^{1}H-NMR (300 MHz, $CDCl_3$, T = 298 K, ppm) δ: 2.17 (s, 3H, =CCH_3), 3.23 (s, 3H, OCH_3), 3.67 (s, 3H, OCH_3), 3.77 (s, 3H, OCH_3), 3.92 (s, 3H, OCH_3), 7.81-7.87 (m, 2H, phen-H^3, phen-H^8), 7.96-7.99 (AB system, J = 8.9 Hz, 2H, phen-H^5, phen-H^6), 8.50-8.55 (m, 2H, phen-H^4, phen-H^7), 9.32 (dd, J = 4.6, 1.4 Hz, phen-H^9), 9.41 (dd, J = 4.6, 1.4 Hz, phen-H^2).
^{13}C{^{1}H}-NMR (T = 298K, $CDCl_3$, ppm) δ: 19.2 (CH_3, =CCH_3), 51.5 (CH_3, OCH_3), 52.1 (CH_3, OCH_3), 52.2 (CH_3, OCH_3), 52.2 (CH_3, OCH_3), 125.0, 125.1 (CH, phen-CH^3, phen-CH^8), 126.9, 127.2 (CH, phen-CH^5, phen-CH^6), 127.3 (C, =CCH_3), 129.6, 129.7 (C, phen-C^{13}, phen-C^{14}), 132.4 (C, C=C), 138.0, 138.2 (CH, phen-CH^4, phen-CH^7), 141.8 (C, C=C), 145.3, 146.9 (C, phen-C^{11}, phen-CH^{12}), 149.6 (CH, phen-CH^9), 154.1 (CH, phen-CH^2), 161.3 (C, CO), 167.3 (C, CO), 167.6 (C, Pd-C=), 170.1 (C, CO), 173.5 (C, CO).
IR (KBr pellet): $\nu_{C=O}$ = 1716, 1728 cm^{-1}
Elemental analysis calcd (%) for $C_{25}H_{23}ClN_2O_8Pd$: C, 48.33, H, 3.73, N, 4.51; found: C, 47.98, H, 3.81, N, 4.60.

Synthesis of [Pd(neocuproine)Cl(C_2(COOMe)$_2$$CH_3$)] (3a)

Complex **3a** was prepared using a similar procedure, starting from 0.0820 g (0.1594 mmol) of the precursor [Pd(Me-PyCH_2SPh)Cl(C_2(COOMe)$_2$$CH_3$)] (**1a**) and 0.0365 g (0.1754 mmol) of neocuproine.
0.0764 g (yield 95%) of **3a** was obtained (yellow microcrystalline powder).

^{1}H-NMR (300 MHz, $CDCl_3$, T = 298 K, ppm) δ: 2.64 (s, 3H, =CCH_3), 3.00 (s, 3H, neoc-CH_3), 3.26 (s, 3H, neoc-CH_3), 3.59 (s, 3H, OCH_3), 3.68 (s, 3H, OCH_3), 7.56-7.63 (m, 2H, neoc-H^3, neoc-H^8), 7.81-7.83 (AB system, J = 8.8 Hz, 2H, neoc-H^5, neoc-H^6), 8.25-8.33 (m, 2H, neoc-H^4, neoc-H^7).
^{13}C{^{1}H}-NMR (T = 298K, $CDCl_3$, ppm) δ: 21.8 (CH_3, =CCH_3), 26.8 (CH_3, neoc-CH_3), 28.5 (CH_3, neoc-CH_3), 51.6 (CH_3, OCH_3), 51.7 (CH_3, OCH_3), 125.5, 125.9 (CH, neoc-CH^3, neoc-CH^8), 126.3, 126.5 (CH, neoc-CH^5, neoc-CH^6), 127.4, 127.5 (C, phen-C^{13}, phen-CH^{14}), 128.7 (C, =CCH_3), 137.5, 138.0 (CH, neoc-CH^4, neoc-CH^7), 145.9, 147.3 (C, neoc-C^{11}, neoc-C^{12}), 150.9 (C, Pd-C=), 162.9 (C, CO), 164.6 (C, neoc-CH^9), 165.9 (C, neoc-CH^2), 172.1 (C,CO).
IR (KBr pellet): $\nu_{C=O}$ = 1697, 1711 cm^{-1}
Elemental analysis calcd (%) for $C_{21}H_{21}ClN_2O_4Pd$: C, 49.72, H, 4.17, N, 5.52; found: C, 50.04, H, 4.07, N, 5.42.

Synthesis of [Pd(neocuproine)Cl(C_4(COOMe)$_4$$CH_3$)] (3b)

Complex **3b** was prepared using a similar procedure, starting from 0.0820 g (0.1249 mmol) of the precursor [Pd(Me-PyCH_2SPh)Cl(C_4(COOMe)$_4$$CH_3$)] (**1b**) and 0.0286 g (0.1374 mmol) of neocuproine.
0.0606 g (yield 75%) of **3b** was obtained (yellow microcrystalline powder). *n*-Hexane/diethylether (1:1) was used instead of diethylether for the precipitation of the title complex.

^{1}H-NMR (300 MHz, $CDCl_3$, T = 298 K, ppm) δ: 2.08 (s, 3H, =CCH_3), 3.18 (s, 6H, neoc-CH_3), 3.32 (s, 3H, O-CH_3), 3.48 (s, 3H, OCH_3), 3.64 (s, 3H, OCH_3), 3.86 (s, 3H, OCH_3), 7.49-7.52 (m, 2H, neoc-H^3, neoc-H^8), 7.85 (bs, 2H, neoc-H^5, neoc-H^6), 8.27 (d, J = 8.4Hz, 2H, neoc-H^4, neoc-H^7).
$^{13}C\{^{1}H\}$-NMR (T = 298K, $CDCl_3$, ppm) δ: 20.8 (CH_3, =CCH_3), 27.0 (CH_3, neoc-CH_3), 28.6 (CH_3, neoc-CH_3), 51.6 (CH_3, OCH_3), 51.7 (CH_3, OCH_3), 51.8 (CH_3, OCH_3), 51.9 (CH_3, OCH_3), 125.4, 125.7 (CH, neoc-CH^3, neoc-CH^8), 125.7, 126.0 (CH, neoc-CH^5, neoc-CH^6), 129.2 (C, =CCH_3), 129.6 (C, C=C), 129.9, (C, phen-C^{13}, phen-CH^{14}), 136.2 (C, C=C), 137.5 (CH, neoc-CH^4, neoc-CH^7), 144.6 (C, neoc-C^{11}, neoc-C^{12}), 155.4 (C, Pd-C=), 162.6 (C, CO), 165.0 (C, neoc-CH^9), 165.0 (C, neoc-CH^2), 162.4 (C, CO), 169.9 (C, CO), 172.2 (C, CO).
IR (KBr pellet): $\nu_{C=O}$ = 1710 cm^{-1}
Elemental analysis calcd (%) for $C_{27}H_{27}ClN_2O_8Pd$: C, 49.94, H, 4.19, N, 4.31; found: C, 50.38, H, 4.05, N, 4.20.

Synthesis of [Pd(dppp)Cl(C_2(COOMe)$_2CH_3$)] (4a)

Complex **4a** was prepared using a similar procedure, starting from 0.0820 g (0.1594 mmol) of the precursor [Pd(Me-PyCH_2SPh)Cl(C_2(COOMe)$_2CH_3$)] (**1a**) and 0.0745 g (0.1754 mmol) of 1,3-bis(diphenylphosphino)propane (dppp).
0.0888 g (yield 78%) of **4a** was obtained (pink microcrystalline powder).

^{1}H-NMR (300 MHz, $CDCl_3$, T = 298 K, ppm) δ: 1.85 (m, 3H, =CCH_3), 1.93-2.66 (m, 6H, CH_2), 3.42 (s, 3H, OCH_3), 3.52 (s, 3H, OCH_3), 7.19-7.93 (m, 30H, Ph).
$^{13}C\{^{1}H\}$-NMR (T = 298K, $CDCl_3$, ppm) selected peaks, δ: 18.8 (CH_3, =CCH_3), 22.1 (CH_2, CH_2 central), 26.1 (dd, CH_2, J_{C-P} = 22.6, 4.9 Hz, PCH_2), 27.9 (dd, CH_2, J_{C-P} = 30.1, 9.0 Hz, PCH_2), 51.0 (CH_3, OCH_3), 51.0 (CH_3, OCH_3), 127.5 (C, =CCH_3), 170.6 (d, C, J_{C-P} = 123.9 Hz, Pd-C=), 163.2 (d, C, J_{C-P} = 15.7, CO), 172.7 (C, CO).
$^{31}P\{^{1}H\}$-NMR (T = 298K, $CDCl_3$, ppm) δ: -5.6 (d, J_{P-P} = 49.1 Hz), 15.3 (d, J_{P-P} = 49.1 Hz)
IR (KBr pellet): $\nu_{C=O}$ = 1702 cm^{-1}
Elemental analysis calcd (%) for $C_{34}H_{35}ClO_4P_2Pd$: C, 57.40, H, 4.96; found: C, 57.17, H, 5.11.

Synthesis of [Pd(dppp)Cl(C_4(COOMe)$_4CH_3$)] (4b)

Complex **4b** was prepared using a similar procedure, starting from 0.0820 g (0.1249 mmol) of the precursor [Pd(Me-PyCH_2SPh)Cl(C_4(COOMe)$_4CH_3$)] (**1b**) and 0.0584 g (0.1374 mmol) of 1,3-bis(diphenylphosphino)propane (dppp).
0.0991 g (yield 93%) of **4b** was obtained (orange microcrystalline powder). *n*-Hexane/diethylether (1:1) was used instead of diethylether for the precipitation of the title complex.

^{1}H-NMR (300 MHz, $CDCl_3$, T = 298 K, ppm) δ: 1.18 (m, 3H, =CCH_3), 2.17-3.00 (m, 6H, CH_2), 3.51 (s, 3H, OCH_3), 3.65 (s, 3H, OCH_3), 3.78 (s, 3H, OCH_3), 3.83 (s, 3H, OCH_3), 7.02-7.86 (m, 30H, Ph).
$^{13}C\{^{1}H\}$-NMR (T = 298K, $CDCl_3$, ppm) selected peaks, δ: 16.4 (CH_3, =CCH_3), 22.1 (CH_2, CH_2 central), 26.1 (dd, CH_2, J_{C-P} = 22.6, 6.4 Hz, PCH_2), 25.9 (dd, CH_2, J_{C-P} = 29.8, 7.2 Hz, PCH_2), 51.4 (CH_3, OCH_3), 51.6 (CH_3, OCH_3), 52.2 (CH_3, OCH_3), 53.1 (CH_3, OCH_3), 164.7 (d, C, J_{C-P} = 14.8, CO), 168.4 (C, CO), 170.2 (C, CO),172.8 (C, CO), (the four signals C=C are not detectable).

$^{31}P\{^{1}H\}$-NMR (T = 298K, $CDCl_3$, ppm) δ: -5.0 (d, J_{P-P} = 45.5 Hz), 11.3 (d, J_{P-P} = 45.5 Hz).
IR (KBr pellet): $\nu_{C=O}$ = 1713 cm^{-1}
Elemental analysis calcd (%) for $C_{40}H_{41}ClO_8P_2Pd$: C, 56.29, H, 4.84; found: C, 56.50, H, 4.73.

Synthesis of [Pd(BnImCH$_2$ImBn)Cl(C$_4$(COOMe)$_4$CH$_3$)] (7b)

Complex **7b** was prepared using a similar procedure, starting from 0.0820 g (0.1249 mmol) of the precursor [Pd(Me-PyCH$_2$SPh)Cl(C$_4$(COOMe)$_4$CH$_3$)] (**1b**) and 0.0767 g (0.1249 mmol) of silver complex **6** (AgBr was removed after 30 min by filtration on millipore membrane filter).
0.0937 g (yield 97%) of **7b** was obtained (brownish microcrystalline powder).

^{1}H-NMR (300 MHz, $CDCl_3$, T = 298 K, ppm) δ: 2.34 (s, 3H, =CCH_3), 3.37 (s, 3H, OCH_3), 3.56 (s, 3H, OCH_3), 3.74 (s, 3H, OCH_3), 3.79 (s, 3H, OCH_3), 4.79-6.29 (AB system, J = 14.8 Hz, 2H, CH_2Ph), 5.09-6.27 (AB system, J = 15.0 Hz, 2H, CH_2Ph), 5.42-6.75 (AB system, J = 13.2 Hz, 2H, NCH_2N), 6.51 (d, J = 2.1 Hz, 1H, CH=CH^{Im}), 6.65 (d, J = 1.9 Hz, 1H, CH=CH^{Im}), 6.90 (d, J = 1.9 Hz, 1H, CH=CH^{Im}), 6.91 (d, J = 2.1 Hz, 1H, CH=CH^{Im}), 7.21-7.35 (10H, Ar-H).
$^{13}C\{^{1}H\}$-NMR (T = 298K, $CDCl_3$, ppm) δ: 20.9 (CH_3, =CCH_3), 51.3 (CH_3, OCH_3), 51.6 (CH_3, OCH_3), 52.2 (CH_3, OCH_3), 54.3 (CH_2, CH_2Ph), 54.9 (CH_2, CH_2Ph), 63.6 (CH_2, NCH_2N), 119.5 (CH, CH=CH^{Im}), 119.8 (CH, CH=CH^{Im}), 120.7 (CH, CH=CH^{Im}), 121.0 (CH, CH=CH^{Im}), 127.0-146.1 (Ar-C, C=C), 163.9 (C, CO), 165.3 (C, CO), 166.0 (C, carbene), 169.6 (C, Pd-C=), 172.6 (C, CO), 175.0 (C, carbene), 175.8 (C, CO).
IR (KBr pellet): $\nu_{C=O}$ = 1713 cm^{-1}
Elemental analysis calcd (%) for $C_{34}H_{35}ClN_4O_8Pd$: C, 53.07, H, 4.58, N, 7.28; found: C, 53.40, H, 4.46, N, 7.19.

Synthesis of *trans*-[Pd(PPh$_3$)$_2$Cl(C$_2$(COOMe)$_2$CH$_3$)] (8a)

Complex **8a** was prepared using a similar procedure, starting from 0.0820 g (0.159 mmol) of the precursor [Pd(Me-PyCH$_2$SPh)Cl(C$_2$(COOMe)$_2$CH$_3$)] (**1a**) and 0.0920 g (0.351 mmol) of triphenylphosphine (PPh_3).
0.1120 g (yield 86%) of **8a** was obtained (pale-yellow microcrystalline powder).

^{1}H-NMR (300 MHz, $CDCl_3$, T = 298 K, ppm) δ: 7.72 (m, 12H, Ar-H), 7.40 (m, 18H), 3.42 (s, 3H, $COOCH_3$), 3.13 (s, 3H, $COOCH_3$), 1.22 (t, J_{H-P} = 1.2 Hz, 3H, =C-CH_3).
$^{13}C\{^{1}H\}$-NMR (T= 298K, $CDCl_3$, ppm) δ: 22.1 (CH_3, =CCH_3), 50.3 (CH_3, OCH_3), 50.7 (CH_3, OCH_3), 127.7-135.0 (Ar-C, =CCH_3, C=C), 164.0 (C, CO), 167.2 (C, Pd-C=), 170.6 (C, CO).
$^{31}P\{^{1}H\}$ NMR ($CDCl_3$, T = 298 K, ppm) δ: 26.0.
IR (KBr pellet): $\nu_{C=O}$ = 1709 cm^{-1}
Elemental analysis calcd (%) for $C_{43}H_{39}ClO_4P_2Pd$: C, 62.71, H, 4.77; found: C, 62.86, H, 4.63.

Synthesis of *trans*-[Pd(PPh$_3$)$_2$Cl(C$_4$(COOMe)$_4$CH$_3$)] (8b)

Complex **8b** was prepared using a similar procedure, starting from 0.1000 g (0.1520 mmol) of the precursor [Pd(Me-PyCH$_2$SPh)Cl(C$_4$(COOMe)$_4$CH$_3$)] (**1b**) and 0.0880 g (0.336mmol) of triphenylphosphine (PPh_3).
0.1370 g (yield 93%) of **9b** was obtained (pale orange microcrystalline powder).

^{1}H-NMR (300 MHz, $CDCl_3$, T = 298 K, ppm) δ: 7.68 (m, 12H, Ar-H), 7.37 (m, 18H), 3.74 (s, 3H, $COOCH_3$), 3.56 (s, 3H, $COOCH_3$) 3.33 (s, 3H, $COOCH_3$), 2.94 (s, 3H, $COOCH_3$), 0.82 (t, 3H, =C CH_3).
^{13}C{^{1}H}-NMR (T= 298K, $CDCl_3$, ppm) δ: 15.4 (CH_3, =CCH_3), 51.0 (CH_3, OCH_3), 51.7 (CH_3, OCH_3), 52.2 (CH_3, OCH_3), 52.3 (CH_3, OCH_3), 127.8-136.5 (Ar-C, C=C), 165.4 (C, Pd-C=), 167.4 (C, CO), 168.0 (C, CO), 168.8 (C, CO), 171.1 (C, CO).
^{31}P{^{1}H} NMR ($CDCl_3$, T = 298, ppm) δ: 20.5.
IR (KBr pellet): $\nu_{C=O}$ = 1709 cm^{-1}
Elemental analysis calcd (%) for $C_{49}H_{45}ClO_8P_2Pd$: C, 60.94, H, 4.70; found: C, 60.69, H, 4.81.

Synthesis of *trans*-[Pd(PTA)$_2$Cl(C$_2$(COOMe)$_2$CH$_3$)] (9a)

Complex **9a** was prepared using a similar procedure, starting from 0.0820 g (0.1594 mmol) of the precursor [Pd(Me-PyCH$_2$SPh)Cl(C$_2$(COOMe)$_2$CH$_3$)] (**1a**) and 0.0526 g (0.3348 mmol) of 1,3,5-triaza-7-phosphaadamantane (PTA).
0.0938 g (yield 96%) of **9a** was obtained (white microcrystalline powder).

^{1}H-NMR (300 MHz, CD_2Cl_2, T = 298 K, ppm) δ: 2.49 (t, J_{HP} = 1.4 Hz, 3H, =CCH_3), 3.68 (s, 3H, OCH_3), 3.79 (s, 3H, OCH_3), 4.25 (s, 12H, NCH_2P), 4.51 (s, 12H, NCH_2N).
^{13}C{^{1}H}-NMR (T= 298K, CD_2Cl_2, ppm) δ: 22.7 (CH_3, =CCH_3), 50.3 (*pseudo*-t, CH_2, NCH_2P), 51.4 (CH_3, OCH_3), 51.5 (CH_3, OCH_3), 73.1 (CH_2, NCH_2N), 125.8 (C, =CCH_3), 157.4 (t, C, J_{C-P} = 10.2 Hz, Pd-C=), 163.2 (C, CO), 172.2 (C, CO).
^{31}P{^{1}H}-NMR (T=298K, CD_2Cl_2, ppm) δ: -59.3.
IR (KBr pellet): $\nu_{C=O}$ = 1709 cm^{-1}
Elemental analysis calcd (%) for $C_{19}H_{33}ClN_6O_4P_2Pd$: C, 37.21, H, 5.42, N, 13.70; found: C, 37.40, H, 5.33, N, 13.58.

Synthesis of *trans*-[Pd(PTA)$_2$Cl(C$_4$(COOMe)$_4$CH$_3$)] (9b)

Complex **9b** was prepared using a similar procedure, starting from 0.0820 g (0.1249 mmol) of the precursor [Pd(Me-PyCH$_2$SPh)Cl(C$_4$(COOMe)$_4$CH$_3$)] (**1b**) and 0.0412 g (0.2623 mmol) of 1,3,5-triaza-7-phosphaadamantane (PTA).
0.0860 g (yield 91%) of **9b** was obtained (pale orange microcrystalline powder).

^{1}H-NMR (300 MHz, $CDCl_3$, T = 298 K, ppm) δ: 1.95 (s, 3H, =CCH_3), 3.74 (s, 3H, OCH_3), 3.82 (s, 3H, OCH_3), 3.83 (s, 3H, OCH_3), 3.89 (s, 3H, OCH_3),4.29 (m, 12H, NCH_2P), 4.51 (m, 12H, NCH_2N).
^{13}C{^{1}H}-NMR (T= 298K, $CDCl_3$, ppm) δ: 17.6 (CH_3, =CCH_3), 50.3 (*pseudo*-t, CH_2, NCH_2P), 50.0 (CH_3, OCH_3), 52.3 (CH_3, OCH_3), 52.6 (CH_3, OCH_3), 52.9 (CH_3, OCH_3), 73.2 (CH_2, NCH_2N), 127.8 (C, =CCH_3), 135.4 (C, C=C), 136.4 (C, C=C), 162.4 (C, CO), 168.1 (C, CO), 168.9 (C, CO), 170.3 (t, C, J_{C-P} = 9.8 Hz, Pd-C=), 172.4 (C, CO).
^{31}P{^{1}H}-NMR (T=298K, $CDCl_3$, ppm) δ: -55.8.
IR (KBr pellet): $\nu_{C=O}$ = 1718 cm^{-1}
Elemental analysis calcd (%) for $C_{25}H_{39}ClN_6O_8P_2Pd$: C, 39.75, H, 5.20, N, 11.12; found: C, 40.01, H, 5.09, N, 11.04.

Synthesis of *trans*-[Pd($AsPh_3$)$_2$Cl(C_2(COOMe)$_2$$CH_3$)] (10a)

Complex **10a** was prepared using a similar procedure, starting from 0.0820 g (0.1594 mmol) of the precursor [Pd(Me-$PyCH_2SPh$)Cl(C_2(COOMe)$_2$$CH_3$)] (**1a**) and 0.1025 g (0.3348 mmol) of triphenylarsine ($AsPh_3$).
0.1272 g (yield 87%) of **10a** was obtained (white microcrystalline powder). *n*-Hexane/diethylether (1:1) was used instead of diethylether for the precipitation of the title complex.

^{1}H-NMR (300 MHz, $CDCl_3$, T = 298 K, ppm) δ: 1.39 (s, 3H, =CCH_3), 3.09 (s, 3H, OCH_3), 3.38 (s, 3H, OCH_3), 7.35-7.46 (m, 18H, Ph), 7.68-7.71 (m, 12H, Ph).
^{13}C{^{1}H}-NMR (T= 298K, $CDCl_3$, ppm) δ: 22.0 (CH_3, =CCH_3), 50.5 (CH_3, OCH_3), 50.9 (CH_3, OCH_3), 128.5 (CH, CH-Ph), 128.6 (C, =CCH_3), 129.9 (CH, CH-Ph), 132.7 (C, C-Ph), 134.2 (CH, CH-Ph), 160.8 (C, Pd-C=), 162.9 (C, CO), 170.7 (C, CO).
IR (KBr pellet): $\nu_{C=O}$ = 1701 cm^{-1}
Elemental analysis calcd (%) for $C_{43}H_{39}As_2ClO_4Pd$: C, 56.66, H, 4.31; found: C, 56.90, H, 4.19.

Synthesis of *trans*-[Pd($AsPh_3$)$_2$Cl(C_4(COOMe)$_4$$CH_3$)] (10b)

Complex **10b** was prepared using a similar procedure, starting from 0.0820 g (0.1249 mmol) of the precursor [Pd(Me-$PyCH_2SPh$)Cl(C_4(COOMe)$_4$$CH_3$)] (**1b**) and 0.0803 g (0.2623 mmol) of triphenylarsine ($AsPh_3$).
0.1202 g (yield 91%) of **10b** was obtained (pale orange microcrystalline powder). *n*-Hexane/diethylether (1:1) was used instead of diethylether for the precipitation of the title complex.

^{1}H-NMR (300 MHz, $CDCl_3$, T = 298 K, ppm) δ: 0.84 (s, 3H, =CCH_3), 2.92 (s, 3H, OCH_3), 3.40 (s, 3H, OCH_3), 3.60 (s, 3H, OCH_3), 3.74 (s, 3H, OCH_3), 7.33-7.44 (m, 20H, Ph), 7.69-7.71 (m, 10H, Ph).
^{13}C{^{1}H}-NMR (T= 298K, $CDCl_3$, ppm) δ: 15.2 (CH_3, =CCH_3), 50.9 (CH_3, OCH_3), 51.8 (CH_3, OCH_3), 52.2 (CH_3, OCH_3), 52.5 (CH_3, OCH_3), 128.4 (CH, CH-Ph), 128.6 (C, =CCH_3), 129.8 (CH, CH-Ph), 133.0 (C, C-Ph), 134.4 (CH, CH-Ph), 135.1 (C, C=C), 136.6 (C, C=C), 163.8 (C, CO), 165.3 (C, Pd-C=), 168.0 (C, CO), 168.7 (C, CO), 171.2 (C, CO).
IR (KBr pellet): $\nu_{C=O}$ = 1697, 1723 cm^{-1}
Elemental analysis calcd (%) for $C_{49}H_{45}As_2ClO_8Pd$: C, 55.86, H, 4.31; found: C, 59.01, H, 4.22.

Synthesis of *trans*-[Pd(PTA)$_2$(C≡C-Ph)(C_2(COOMe)$_2$$CH_3$)] (13)

0.0795 g (0.1297 mmol) of **9a** was dissolved in 7 mL of anhydrous dichloromethane in a 50 mL two-necked flask under inert atmosphere (Ar). Subsequently, 0.0670 g (60 µL, 0.1712 mmol) of [(PhC≡C)Sn(*n*-Bu)$_3$] was added. The mixture was stirred at room temperature for 3 hours and the solvent was then removed under vacuum. The final product (white microcrystalline powder) was triturated with *n*-hexane/diethylether (1:1) and filtered off on a gooch filter.
0.0828 g of **13** was obtained (yield 94%).

^{1}H-NMR (300 MHz, CD_2Cl_2, T = 298 K, ppm) δ: 2.03 (t, J_{H-P} = 1.3 Hz, 3H, =CCH_3), 3.67 (s, 3H, OCH_3), 3.74 (s, 3H, OCH_3), 4.33 (s, 12H, NCH_2P), 4.54 (s, 12H, NCH_2N), 7.21-7.40 (m, 5H, Ph).

$^{13}C\{^1H\}$-NMR (T = 298K, $CDCl_3$, ppm) δ: 22.7 (CH_3, $=CCH_3$), 51.1 (CH_3, OCH_3), 51.6 (CH_3, OCH_3), 52.0 (*pseudo*-t, CH_2, NCH_2P), 73.3 (CH_2, NCH_2N), 101.4 (t, C, J_{C-P} =23.1Hz, ≡C-Pd), 115.0 (C, ≡C-Ph), 126.2 (CH, CH-Ph), 126.6 (C, $=CCH_3$), 126.7 (C, C-Ph), 128.2 (CH, CH-Ph), 131.1 (CH, CH-Ph), 163.9 (C, CO), 168.0 (t, C, J_{C-P} = 11.1 Hz, Pd-C=), 175.3 (C, CO).
$^{31}P\{^1H\}$-NMR (T=298K, CD_2Cl_2, ppm) δ: -58.5.
IR (KBr pellet): $\nu_{C=O}$ = 1701, $\nu_{C\equiv C}$ = 2100 cm^{-1}
Elemental analysis calcd (%) for $C_{27}H_{38}ClN_6O_4P_2Pd$: C, 47.76, H, 5.64, N, 12.38; found: C, 47.50, H, 5.73, N, 12.51.

Cell viability assay

Cells were grown in agreement with the supplier and incubated at 37°C (5% of CO_2). 1.5 x 10^3 cells were plated in 96 wells and treated with six different concentrations of palladium compounds (0.001, 0.01, 0.1, 1, 10, and 100 µM). After 96 hours, cell viability was evaluated with CellTiter glow assay (Promega, Madison, WI, USA) with a Tecan M1000 instrument. IC_{50} values were obtained from triplicates, and error bars are standard deviations.

PDTOs culture and viability assay

Specimens were completely de-identified prior to use, and consent for research utilization was secured through the biobank at the National Cancer Institute (CRO) in Aviano.
Clusters of cells from ascites was isolated by spinning at 1,000 rpm for 10 minutes and then washed twice with two rounds of HBSS (Gibco, Massachusetts, United States). To remove erythrocytes, the samples were treated with a chilled erythrocyte lysis solution (Roche Diagnostics, Basel, Switzerland) while stirring on ice for 10 minutes. After another centrifugation at 1,000 rpm for 10 minutes, the resulting cell pellet was suspended in Geltrex™ Reduced Growth Factor Basement Membrane Matrix (Gibco, Massachusetts, United States). For solid tumors, the protocol included a 30-minutes incubation in a cocktail of antibiotics and antifungal agents in Dulbecco's Modified Eagle Medium/Nutrient Mixture F-12 Ham, followed by mincing into 0.5–1 mm^3 fragments and enzymatic dissociation using a 4 mg/mL collagenase IV (Gibco, Massachusetts, United States) solution at 37°C for a maximum of 45 minutes. The resulting clusters of cells were again spun down, reconstituted in Geltrex™ Reduced Growth Factor Basement Membrane Matrix, and plated in a 24-well format. Following Geltrex™ solidification, the organoids were maintained in a specialized medium as specified by Kopper et al., refreshed triweekly, and incubated at 37°C with a 5% CO_2 atmosphere.[4] Clusters of organoids were mixed in an appropriate volume of Geltrex™ Reduced Growth Factor Basement Membrane matrix and 2 µL of this mixture was seeded in 96-wells plates in four replicates. The organoids were treated with six different concentrations of carboplatin and compound **9b**. After 96 h, cell viability was measured using CellTiter-Glo 3D (Promega, Madison, WI, United States). The luminescence was acquired with BioTek Synergy H1 instrument.

ROS production

A2780 and OVCAR5 cells were plated in a 96-well plate at a concentration of $1.5 \cdot 10^3$ cells per well. Cells were treated at the predetermined time points (24, 48, and 96 hours) with compound **9b** at concentrations of 1, 25, and 50 µM. Doxorubicin at 1 µM was used as a positive control. After 96 hours from the seeding, ROS production was evaluated using the ROS-Glo™ H_2O_2 Assay (catalog no. G8821, Promega) with BioTek Synergy H1 instrument.

Caspases activity

A2780 and OVCAR5 cells were plated in a 96-well plate at a concentration of $1.5 \cdot 10^3$ cells per well. Cells were treated at the predetermined time points (24, 48, and 96 hours) with compound **9b** at concentrations of 1, 25, and 50 µM. Doxorubicin at 1 µM was used as a positive control. After 96 hours from the seeding, ROS production was evaluated using the Caspase-Glo® 3/7 Assay (catalog no. G8090, Promega) with BioTek Synergy H1 instrument.

Cytochrome C release assay

To assess the release of cytochrome C from the mitochondrial membrane, OVCAR-5 cells were seeded on 8-well chamber slides (20000 cells per well). Cells were placed in incubator overnight (37 °C, 5% CO_2) and then treated with compound **9b** at the concentration 0.1 µM, 1 µM and 10 µM for 3, 6, 24, 48, 72 and 96 hours. A negative and a positive controls (for positive control, cisplatin at the concentration 10 µM was used) were considered for each timepoint. At the end of the treatment, the medium was removed from each well and cells were fixed in 4% paraformaldehyde (DPBS solution; incubation for 20 min at room temperature), permeabilized with a 3% solution of Triton-X-100 in DPBS (incubation for 15 min at room temperature) and then blocked in 8% BSA (DPBS solution; incubation for 1 h at room temperature). Cells were subsequently incubated overnight with a 1% BSA solution in DPBS with the primary antibody (Cytochrome C (6H2.B4) Mouse mAb, cat. #12963, Cell Signaling, Danvers, MA, USA) (1:100 dilution). Each well was washed three times with DPBS and then the secondary antibody (Goat anti-Mouse IgG (H+L) Highly Cross-Adsorbed Secondary Antibody, Alexa Fluor™ Plus 488, cat. # A32723, Invitrogen, Waltham, MA, USA) was added (1:1000 dilution in 1% BSA solution in DPBS). After 1 h of incubation, cells were washed three times with DPBS and subsequently stained with DAPI 0.1 µg/mL (DBPS solution; incubation for 1 min at room temperature) to visualize nuclei. Cells were washed three times with DPBS and finally the slides were mounted with a mounting solution (FluorSave™ Reagent, cat. # 345789, Millipore, Burlington, MA, USA). Each slide was examined using the confocal microscope NIKON Eclipse TI2 (equipped with X-Light V2 L-FOV spinning disk and lumencore lamp) and the fluorescent images were analysed with NIS software.

Proteomic Analysis

Proteins were extracted from a minimum of $5 \cdot 10^6$ ovarian cancer cells belonging to the following groups: (i) NT and (ii) 1 µM with a lysis buffer (Thermo Fisher Scientific, Massachusetts, USA) containing Universal Nuclease (Thermo Fisher Scientific), 1 x protease inhibitor cocktail (Thermo

Fisher Scientific) and 0.1% (w/v) RapiGest SF (Waters, Massachusetts, USA). Protein concentration was measured with the Pierce BCA Protein Assay Kit (Thermo Fisher Scientific). Protein extracts were immediately subjected to further down-stream analyses.

Briefly, proteins (100 µg) were reduced, alkylated and digested and peptides cleaned-up with the EasyPep Mini MS Sample Prep Kit (Thermo Fisher Scientific) according to the manufacturer's protocol. The extracted peptides were lyophilized and then resuspended in 50 µL of 0.1% formic acid before analysis by LC-MS/MS. Peptide concentration was measured with the Pierce BCA Protein Assay Kit (Thermo Fisher Scientific). Three biological replicates were analyzed per group.

The digested peptide mixtures were analyzed with LC-MS/MS, using a Q-Exactive Plus Hybrid Orbitrap mass spectrometer equipped with a UHPLC Vanquish (Thermo Fisher Scientific). Individual samples (loading amount 15 µg) were analyzed in duplicate. Each peptide sample was fractionated in a XBridge Peptide BEH C18 column (3.5 µm 2.1 x 150, Waters, Sesto San Giovanni, Milan, Italy) at a total flow rate of 200 µL/min using 0.1% formic acid/acetonitrile gradient over a period of 61.5 min and sprayed onto the mass spectrometer using a heated electrospray source probe in positive mode (Thermo Fisher Scientific). Acetonitrile, formic acid and water, all LC-MS grade, were purchased from Sigma Aldrich Srl (Milan, Italy). The mass spectrometer was run in a data-dependent mode with positive polarity. The full scan was performed between 375 and 1500 m/z followed by MS/MS scans on the top 10 intense ion. Raw MS files were analysed and searched against the human database (UniProt release 2022_02) using Proteome Discoverer software (version 2.5.0.400) and its Sequest search engine. Relative protein amount across our samples was determined for most of the identified proteins through label-free quantification (LFQ). Only proteins identified with a high false discovery rate (FDR) (1%), Score Sequest>1 and unique peptides>1 were considered. All potential contaminants coming from culture media were filtered. The abundance ratio (or fold change, FC) of statistically significant proteins was calculated as the ratio of the average LFQ values between the two matched groups. Proteins differing in abundance between the two groups were defined as those with a FC≥2 (FC Log2≥1) (proteins increasing in abundance) or a FC≤2 (FC Log2≤-1) (proteins decreasing in abundance), grouped abundances CV (%) < 30 and FC $P_{adjusted}$ <0.05.

In vivo experiments

Animal experiments were approved by the National Ethical Committee and the Administration of the Republic of Slovenia for Food Safety, Veterinary and Plant Protection (permission no. U34401-33/2019/19). Mice from Envigo were housed in filtertop cages (2–5 per cage) with bedding and enrichment materials (paper towel) and under controlled conditions of temperature (22 ± 2 ˚C), humidity (55 ± 10%), and light (12 h/12 h light–dark cycle) with unlimited access to food and water.

Tumor induction

OVCAR5 cells were cultured, harvested after trypsinization, and suspended in a saline solution enriched with 30% Matrigel HC (Corning) to a density of $3 \cdot 10^7$ cells/mL. Subsequently, 100 µL of this suspension was subcutaneously injected into the flank of mice. The mice were maintained under specific pathogen-free conditions in a carousel mouse IVC rack system (Animal Care Systems Inc.,

USA), with environmental controls set to 55 ± 10% humidity and temperatures between 20–24 °C, under a 12-hour light/dark cycle. They had continuous access to sterile food and water.

Efficacy study

Upon reaching a volume of 100 mm^3, tumor-bearing mice were assorted into different groups: a control group (CTRL), a cisplatin treatment group (CIS), and a group receiving compound **9b** (9b). The treatments were administered intravenously in 100 µL volumes, with cisplatin dosed at 1 mg/kg and **9b** at 100 mg/kg, on days 0, 6, 9, 12, 16, 20, 23, 27, 31, and 34. Tumor sizes were measured three times weekly using Vernier calipers, and volumes calculated using the formula V = ½(Length × $Width^2$). To evaluate tumor growth delay, we identified the time it took for each tumor to double in size from its volume at the start of treatment. We then determined the tumor growth delay for each tumor by deducting its individual tumor doubling time from the average doubling time of the control group's tumors. The average tumor growth delay was calculated for each treatment group. Animal well-being was monitored during the experiment by weighing the animal and visual inspection.

XRD analysis

2a, **2b**, **3b**, **5a** and **13** crystals data were collected at the XRD1 and XRD2 beamlines of the Elettra Synchrotron, Trieste (Italy),[5] using a monochromatic wavelength of 0.620 Å, at 100K. The data sets were integrated, scaled and corrected for Lorentz, absorption and polarization effects using XDS package.[6] Data from two random orientations have been merged to obtain complete datasets for the triclinic **2a**, **2b**, **3b** and **13** crystal forms, using CCP4-Aimless code.[7] The structures were solved by direct methods using SHELXT program[8] and refined using full−matrix least−squares implemented in SHELXL−2018/3.[9]

Thermal motions for all non−hydrogen atoms have been treated anisotropically and hydrogens have been included on calculated positions, riding on their carrier atoms. Geometric and thermal restrains (SAME, FLAT, SIMU) have been applied to disordered fragments in **13**. The Coot program was used for structure building.[10] The crystal data are given in Table S1. Pictures were prepared using Ortep3[11] and Pymol[12] softwares.

Crystallographic data have been deposited at the Cambridge Crystallographic Data Centre and allocated the deposition number CCDC 2343666, 2343667, 2343668, 2343670 and 2343669 for **2a**, **2b**, **3b**, **5a** and **13**, respectively. These data can be obtained free of charge via https://www.ccdc.cam.ac.uk/structures.

Reactivity of Pd(II)-vinyls towards [(PhC≡C)Sn(n-Bu)$_3$]

The extrusion of the vinyl fragment was carried out by reacting the synthesized vinyl complexes with [(PhC≡C)Sn(*n*-Bu)$_3$]. It should be remembered that stannanes are widely used to remove organic residues from a metal center. This process is divided into two steps: transmetallation and subsequent reductive elimination (Scheme S1).

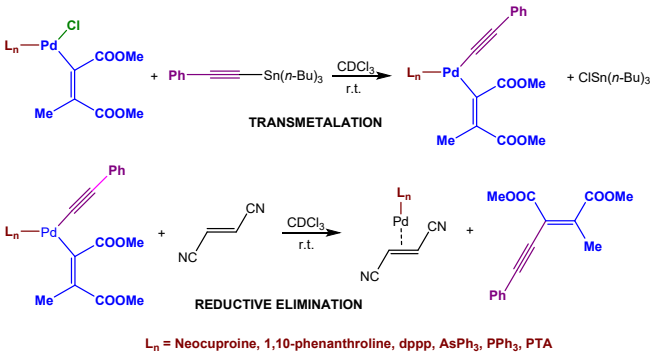

Scheme S1. Transmetalation and reductive elimination steps involved in the reaction between Pd(II)-vinyl complexes and stannanes.

We have chosen to study only the vinyl derivatives since, from preliminary tests we have verified that their butadienyl congeners react much more slowly. Furthermore, [(PhC≡C)Sn(*n*-Bu)$_3$] was chosen as it is known to efficiently promote the release of the phenylethynyl fragment in the transmetallation process.

The addition of fumaronitrile in the reactivity study allows the stabilization of the resulting Pd(0) complex, avoiding the formation of metallic palladium which could trigger parasitic reactions and/or perturb the system during the NMR analysis. The coordination of fumaronitrile has been demonstrated to be faster than the two reactions that precede it. In fact, the rate of the entire process is independent of the concentration of added olefin.

All reactions were monitored by ^{1}H NMR spectroscopy, using a $1.82 \cdot 10^{-2}$ M CD_2Cl_2 solution of the complex, 1.1 equivalents of [(PhC≡C)Sn(*n*-Bu)$_3$] and an excess of fumaronitrile (3.7 equiv.).

The results obtained, expressed as half-life (min) of the initial complex, are reported in Table S1.

Table S1. Half-life ($t_{1/2}$) of Pd(II)-vinyl complexes in the reaction with [(PhC≡C)Sn(*n*-Bu)$_3$].

Complex	Ligand	$t_{1/2}$
2a	1,10-Phenanthroline	18 min
3a	Neocuproine	6 min
4a	1,3-bis(diphenylphosphino)propane	> 24 h
8a	triphenylphosphine	120 min
9a	1,3,5-triaza-7-phosphaadamantane	9 min
10a	triphenylarsine	54 min

From the $t_{1/2}$ values obtained it is evident that the two most reactive complexes are those containing 1,10-phenanthroline and neocuproine (**2a** and **3a**). This high reactivity is probably due to the reduced steric demand of the N-N ancillary ligand, allowing easy access of stannane above and below the main coordination plane. On the contrary, the use of a chelating diphosphine such as dppp results in considerably disadvantage the process. The low reactivity of complex **4a** is due both to the higher steric hindrance of dppp compared to the phenanthroline-based ligands and to the stronger bond that this diphosphine forms with palladium. Considering this latter aspect, it is difficult to easily free coordination sites, a condition that may be required at some stage of the process.

The complexes coordinating two PPh_3 or $AsPh_3$ ligands have an intermediate reactivity between derivatives **2a**/**3a** and **4a**. The lower reactivity compared to complexes containing bidentate N-N ligands is probably due to the need to promote the isomerization of the *trans* transmetallation intermediate in its *cis* congeners, enabling the reductive elimination process.

Curiously, in the case of complex **9a** which coordinates two PTA ligands, the reaction with [(PhC≡C)Sn(*n*-Bu)$_3$] ends with the transmetallation step, without evolving over time with the extrusion of the organic fragment. This means that the intermediate species is particularly stable and does not undergo *trans*/*cis* isomerization, which is crucial for allowing the final reductive elimination step. Based on this evidence, the synthesis of intermediate **13** was carried out in dichloromethane, with a reaction time of 3 hours at room temperature.

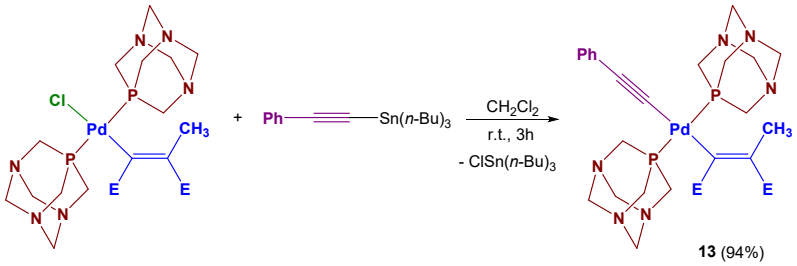

Scheme S2. Synthetic procedure leading to complex **13**.

The ^{31}P NMR spectrum of **13** shows a singlet at -58.5 ppm, confirming the *trans* configuration of the transmetallation product. This conclusion can also be inferred from the ^{1}H and ^{13}C NMR spectra, where only one set of methylene protons/carbons (NCH_2N and NCH_2P), slightly shifted with respect to the starting material, can be detected. Furthermore, all the signals attributable to alkynyl protons and carbons are observable. In particular, the alkynyl carbon directly bound to palladium resonates as a triplet ($J_{C\text{-}P}$ = 23.1 Hz) at 101.4 ppm, whereas that bound to the phenyl substituent appears as a singlet at 115 ppm. In the IR spectrum, the C≡C stretching band at 2100 cm^{-1} is particularly worthy of mention. Finally, the atom connectivity was unambiguously established by single crystal X-ray diffraction (see Crystal structure determination section).

Biological data

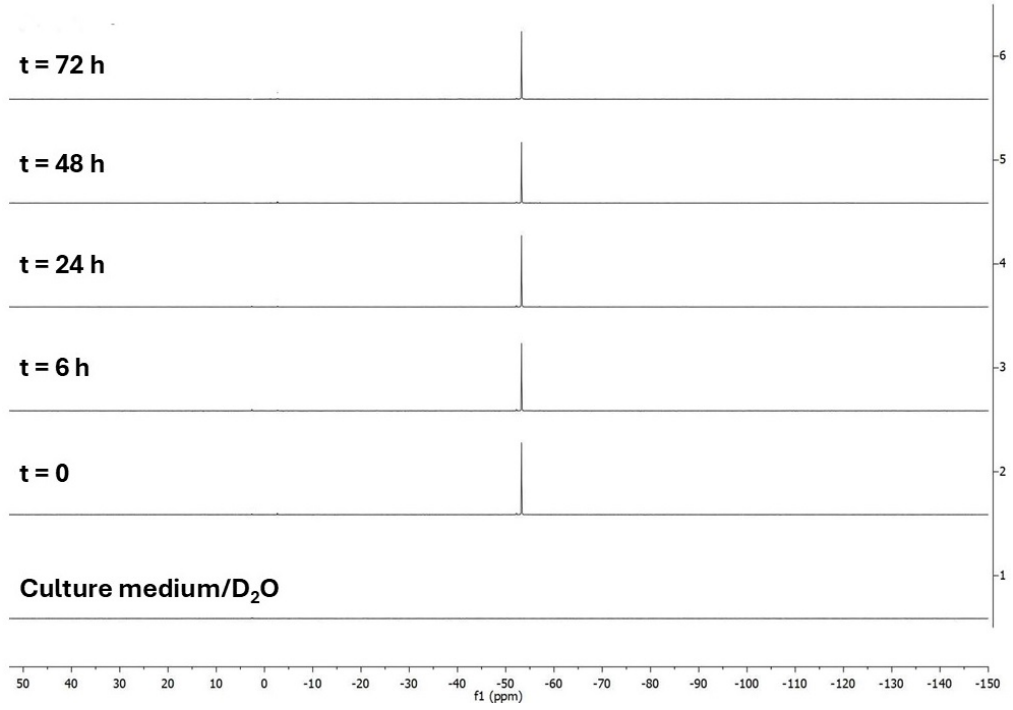

Figure S1: ^{1}H NMR of **9b** in culture medium/D_2O (1:1) at different time points.

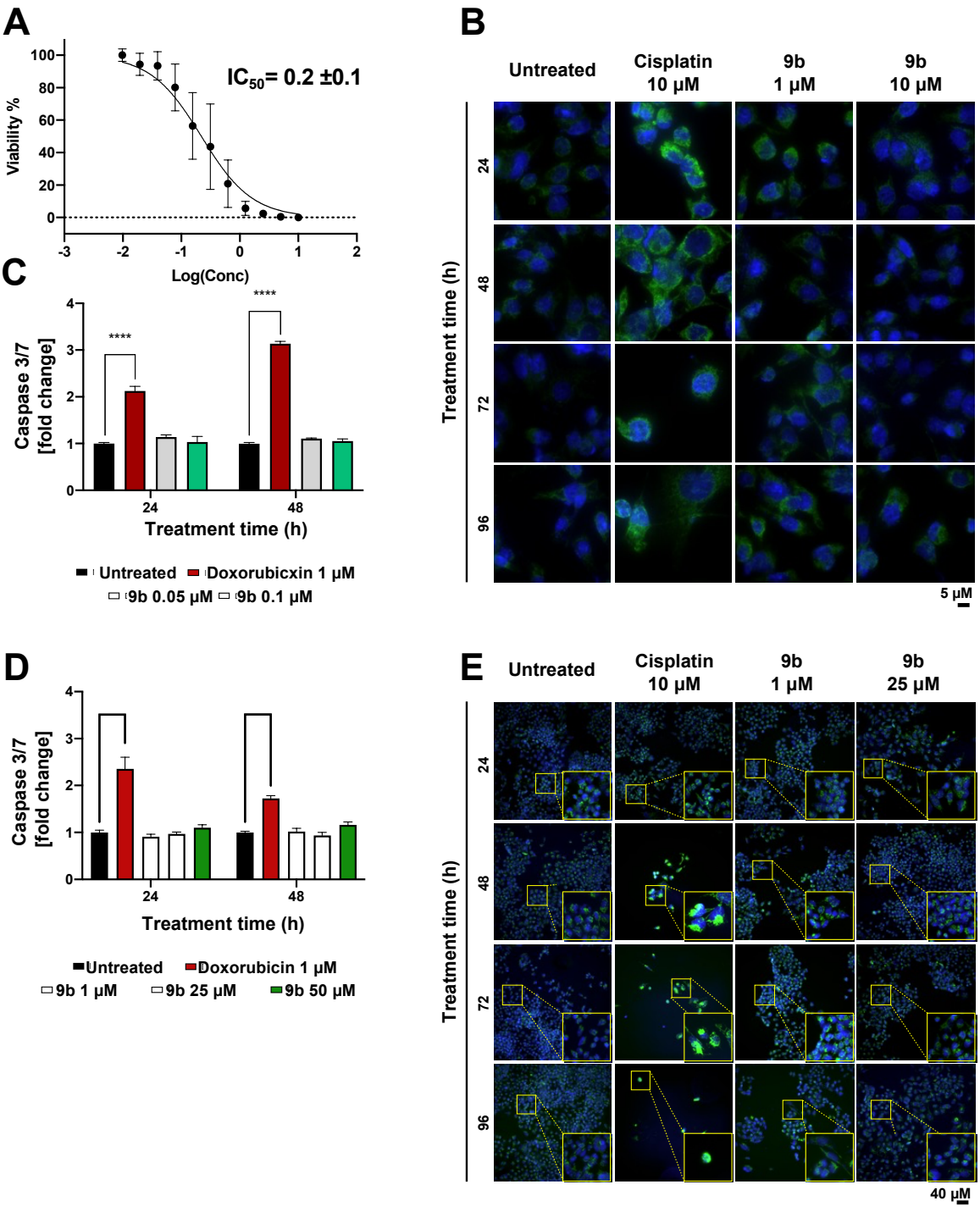

Figure S2: IC_{50} *(**A**) Dose–response curve of OVCAR5 treated with Compound 9b. Dots represent the mean of nine replicates. Error bars represent the SD. IC_{50} value is reported in the graph; (**B**) Immunofluorescence analysis of cytochrome C release on OVCAR5 after 24, 48, 72 and 96 h of treatment with Compound* ***9b*** *and cisplatin as positive control; (**C**)* Caspases 3/7 activation in OVCAR5 and (**D**) A2780 cells treated with compound **9b** (1, 25, 50 µM) and Doxorubicin (1 µM as positive control) at 24 and 48-hour intervals; (**E**) *Immunofluorescence analysis of cytochrome C release on A2780 after 24, 48, 72 and 96 h of treatment with Compound* ***9b*** *and cisplatin as positive control.*

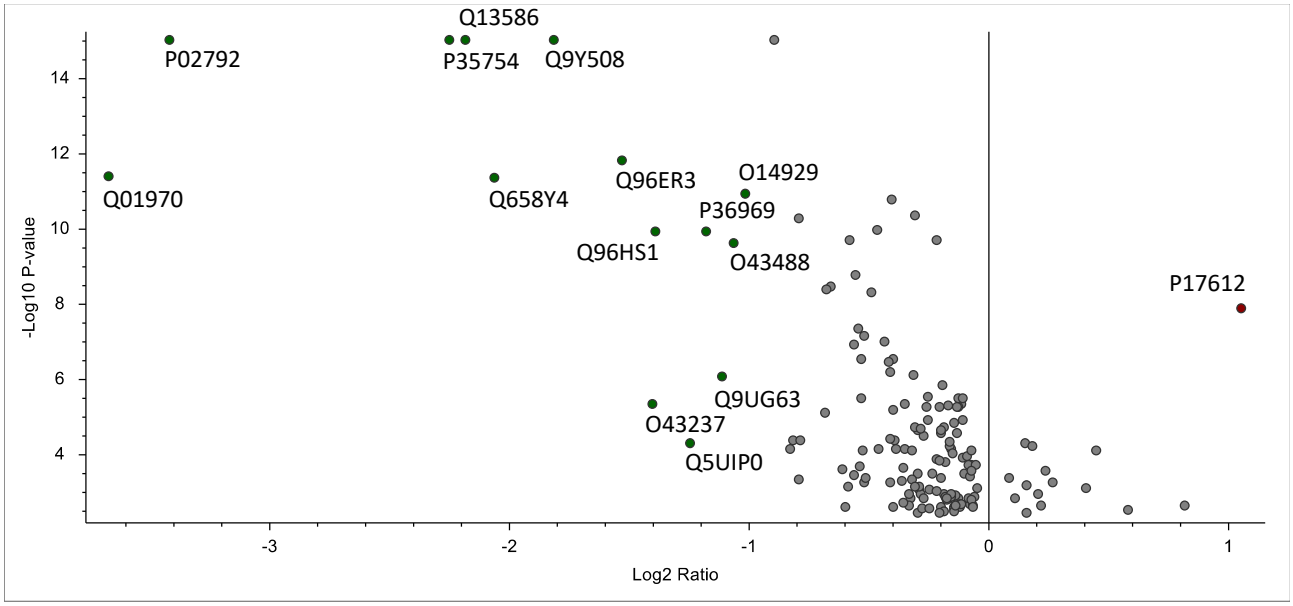

Figure S3: Volcano plot showing proteomic data by cell treatment (1 µM versus NT). Log2 transformed abundance ratios for each protein are plotted on the x-axis. Negative log10 transformed p-values are plotted on the y-axis. Proteins significantly more abundant and less abundant are represented as red and green circles, respectively, 1 µM treated groups than in NT groups. The red and green panels evidence areas containing proteins significantly different for $P_{adj.}$<0.05 and Log_2FC >1 or <-1, respectively. Protein gene names are indicated.

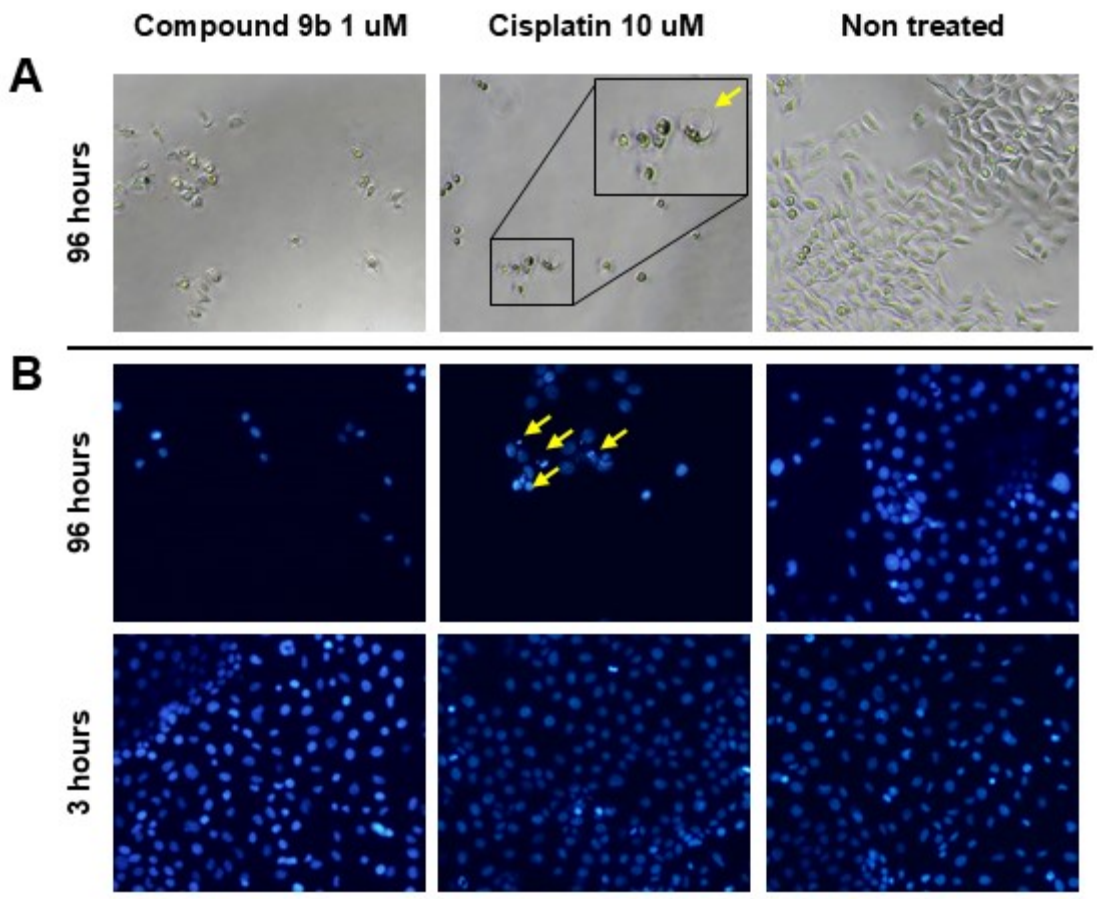

Figure S4: Bright field image (A) and nuclear staining of Ovcar-5 cells with Hoechst 33342 (B) following treatment with Compound **9b** at 1 µM and cisplatin at 10 µM as a positive control for 3 and 96 hours, respectively, compared to untreated cells. Yellow arrows indicate the presence of cellular blebbing and nuclear atypia following cisplatin treatment, which are not observed after treatment with Compound **9b**.

NMR spectra

^{1}H NMR, $^{13}C\{^{1}H\}$ NMR spectra of [Pd(1,10-phen)Cl(C_2(COOMe)$_2$$CH_3$)] (2a)

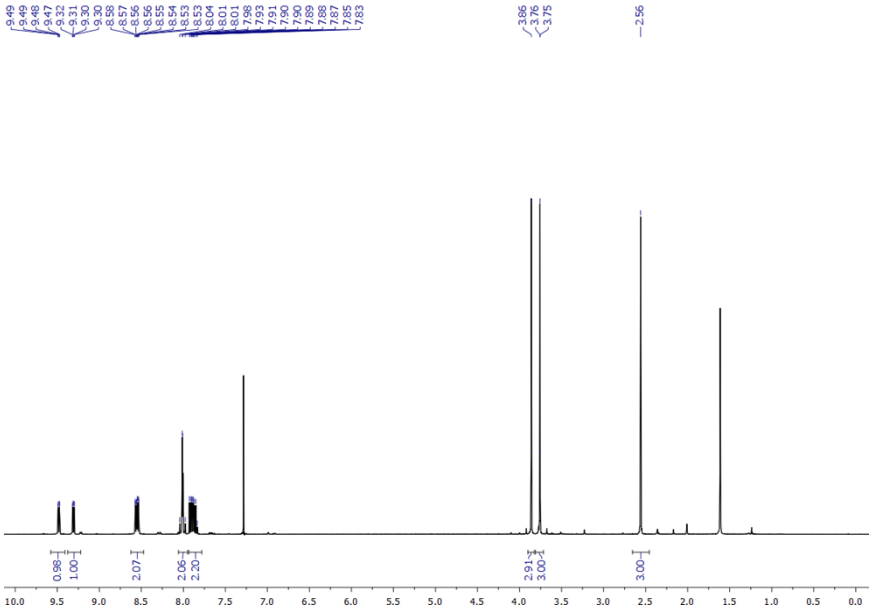

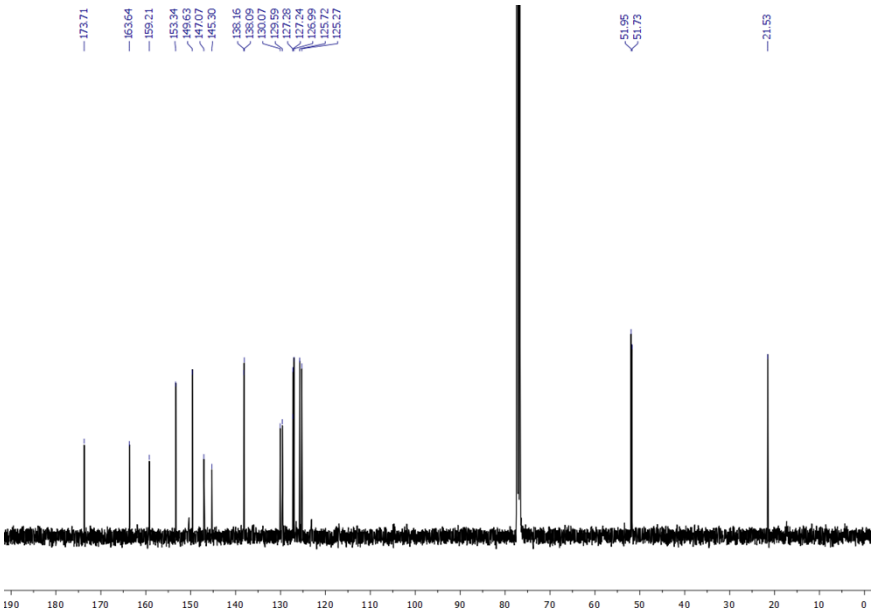

^{1}H NMR, ^{13}C{^{1}H} NMR spectra of [Pd(1,10-phen)Cl(C_4(COOMe)$_4$$CH_3$)] (2b)

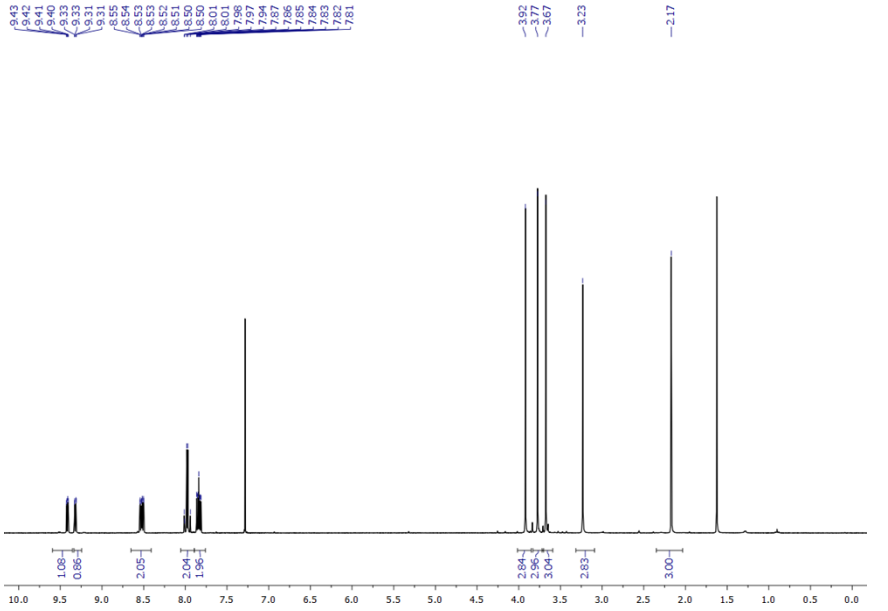

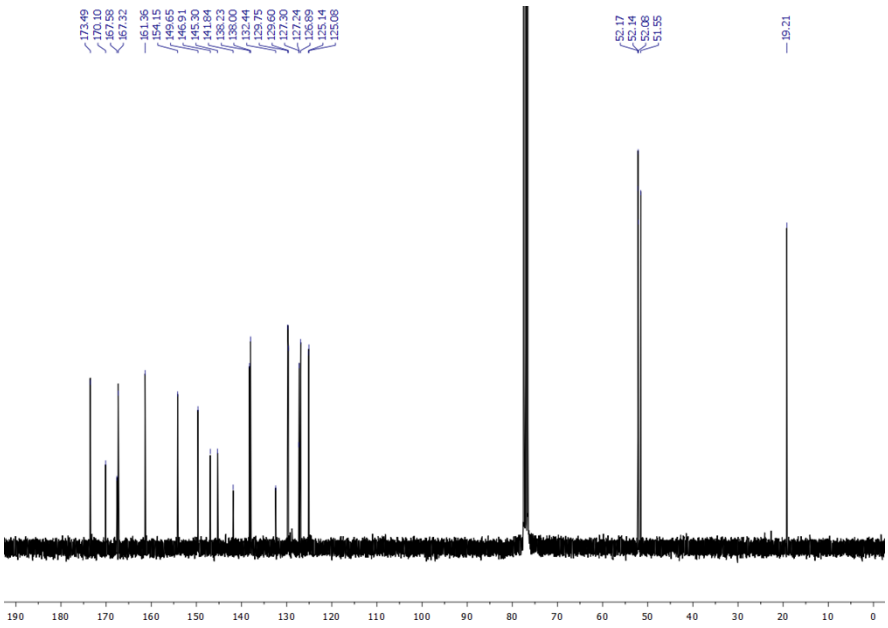

^{1}H NMR, ^{13}C{^{1}H} NMR spectra of [Pd(neocuproine)Cl(C_2(COOMe)$_2$$CH_3$)] (3a)

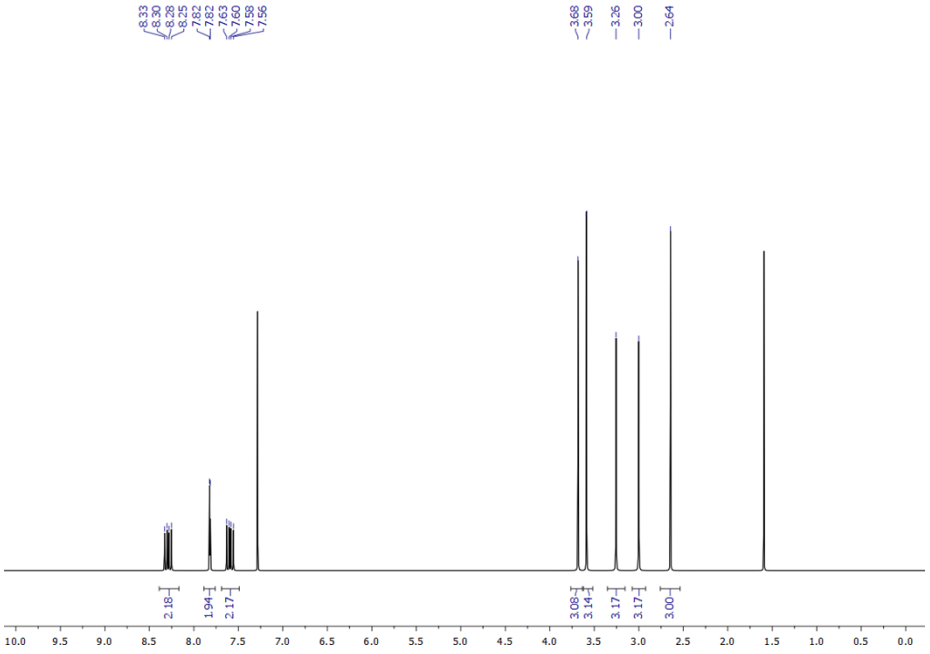

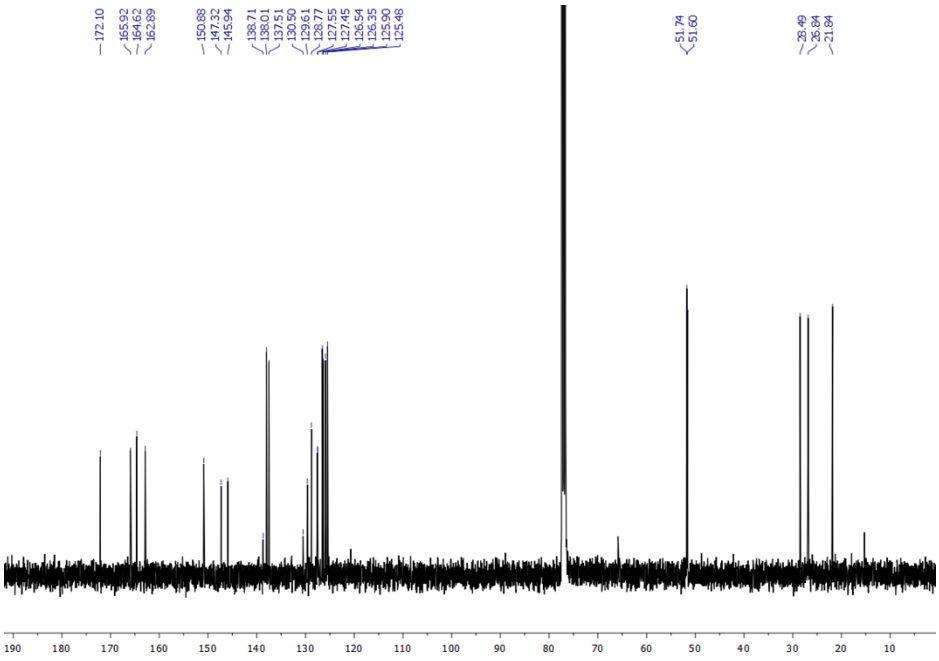

^{1}H NMR, $^{13}C\{^{1}H\}$ NMR spectra of [Pd(neocuproine)Cl(C_4(COOMe)$_4$$CH_3$)] (3b)

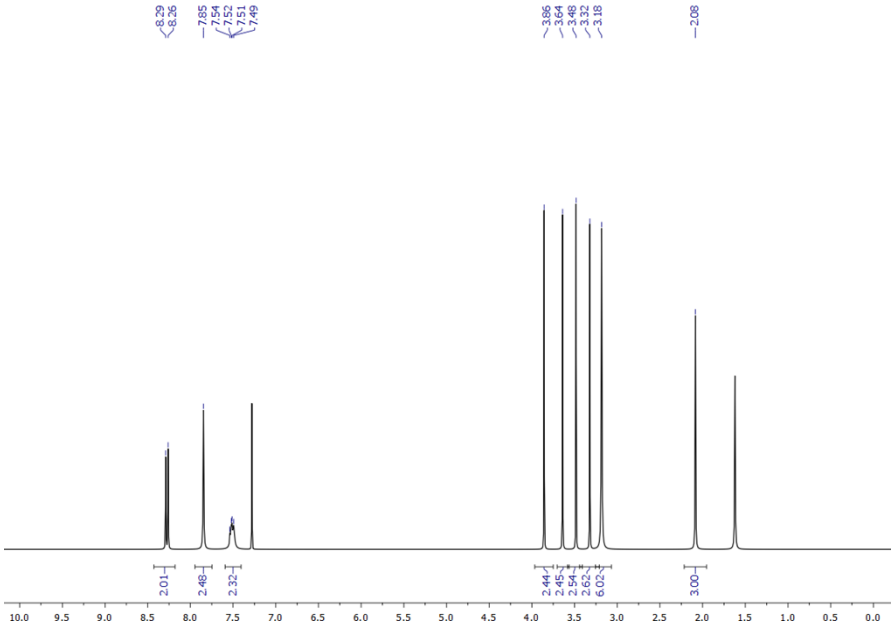

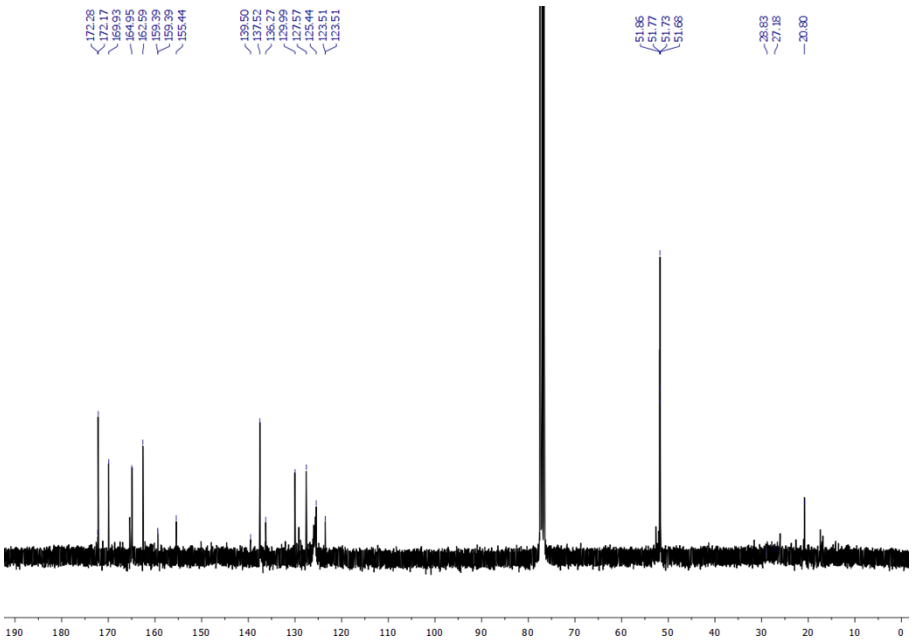

^{1}H NMR, ^{31}P{^{1}H} NMR and ^{13}C{^{1}H} NMR spectra of [Pd(dppp)Cl(C_2(COOMe)$_2$$CH_3$)] (4a)

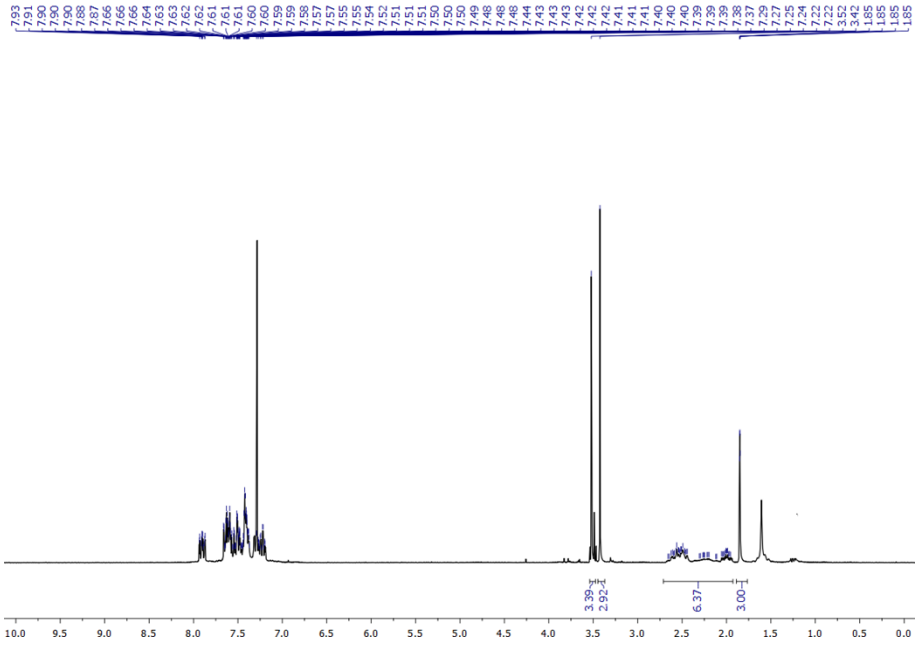

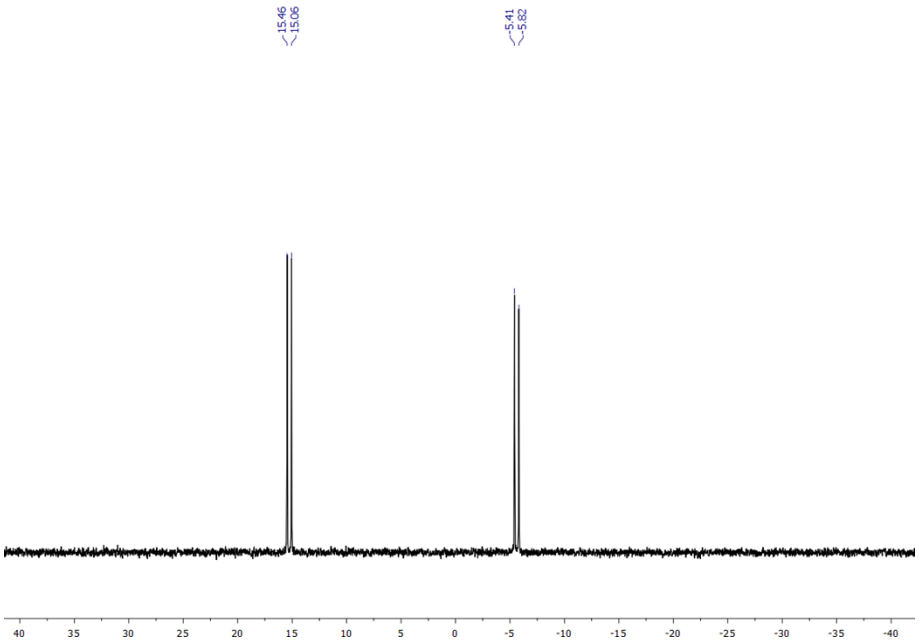

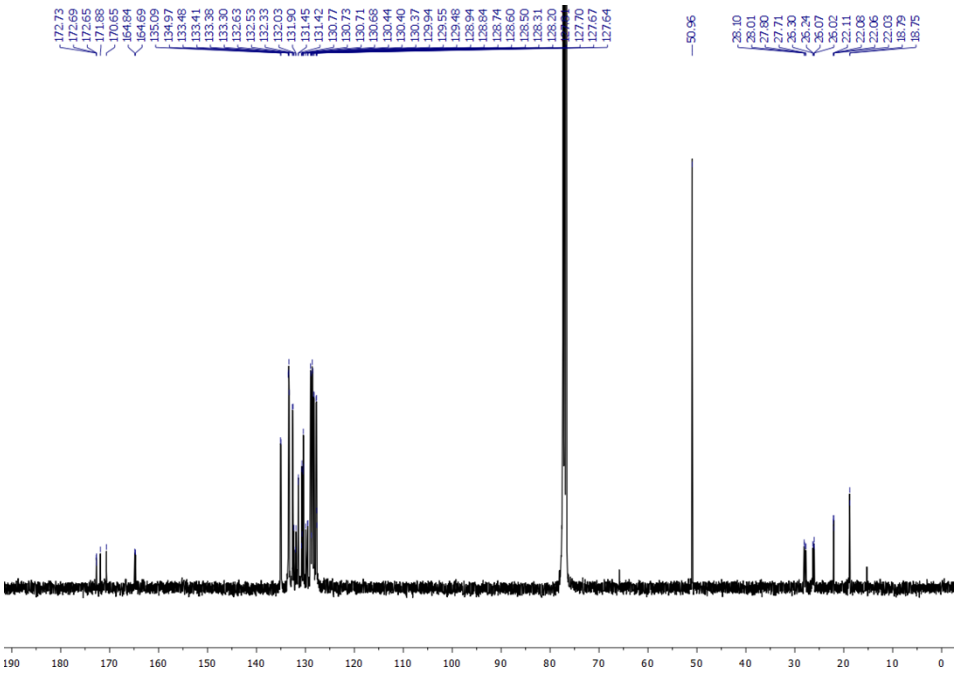
172.73
172.69
172.65
171.88
170.65
164.84
164.69
135.09
134.97
133.48
133.41
133.38
133.30
132.63
132.53
132.33
132.03
131.90
131.45
131.42
130.77
130.73
130.71
130.68
130.44
130.40
130.37
129.94
129.55
129.48
128.94
128.84
128.74
128.60
128.50
128.31
128.20
127.70
127.67
127.64
50.96
28.10
28.01
27.80
27.71
26.30
26.24
26.07
26.02
22.11
22.08
22.06
22.03
18.79
18.75
190
180
170
160
150
140
130
120
110
100
90
80
70
60
50
40
30
20
10
0

^{1}H NMR, $^{31}P\{^{1}H\}$ NMR and $^{13}C\{^{1}H\}$ NMR spectra of [Pd(dppp)Cl(C_4(COOMe)$_4$$CH_3$)] (4b)

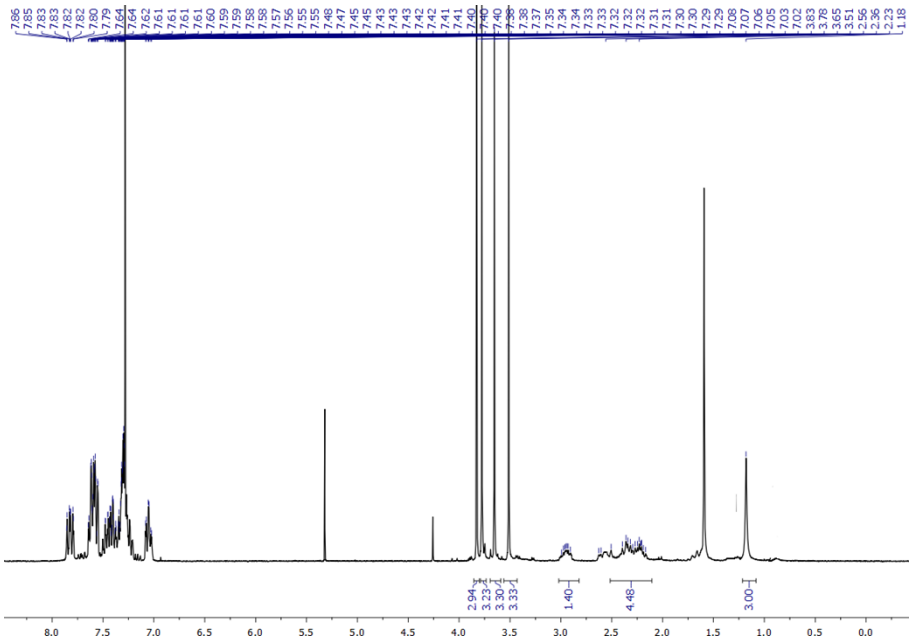

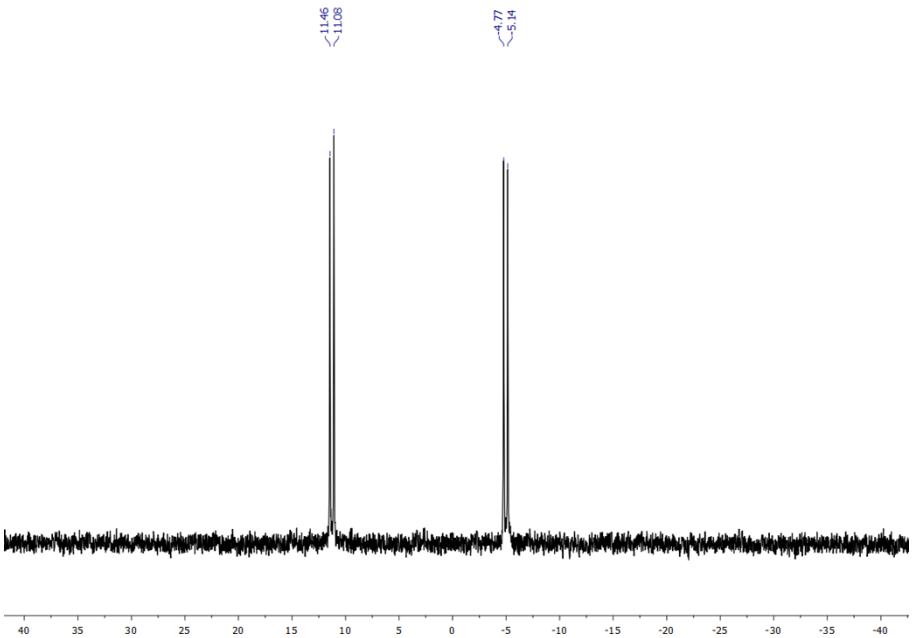

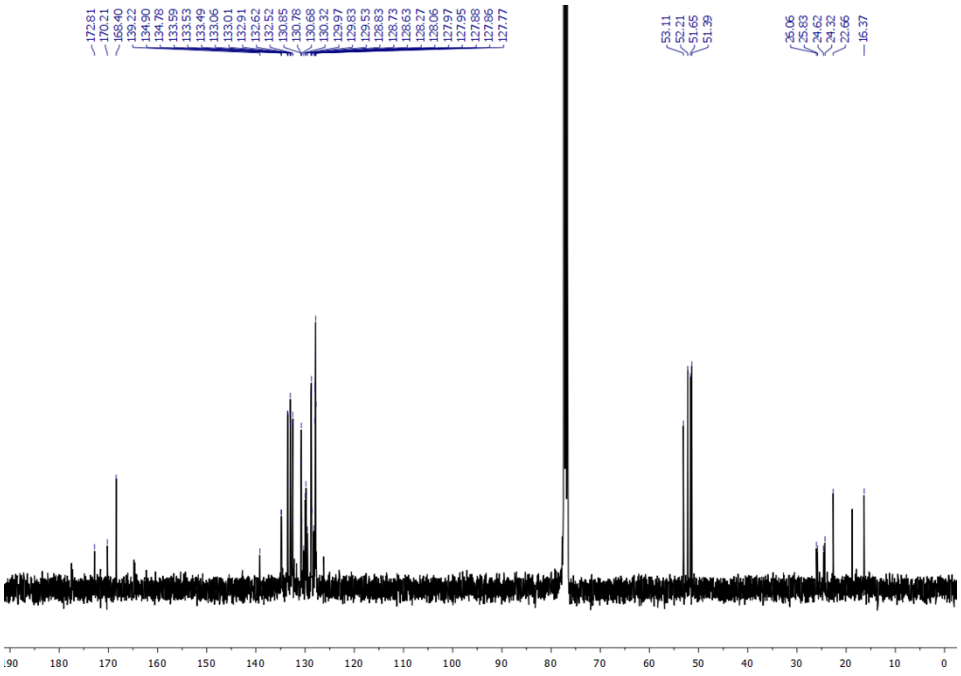
172.81
170.21
166.40
139.22
134.90
134.78
133.59
133.53
133.49
133.06
133.01
132.91
132.62
132.52
130.85
130.78
130.68
130.32
129.97
129.83
129.53
128.83
128.73
128.63
128.27
128.06
127.97
127.95
127.88
127.86
127.77
53.11
52.21
51.65
51.39
26.06
25.83
24.62
24.32
22.66
16.37
190
180
170
160
150
140
130
120
110
100
90
80
70
60
50
40
30
20
10
0

^{1}H NMR, $^{13}C\{^{1}H\}$ NMR spectra of [Pd(BnImCH$_2$ImBn)Cl(C$_4$(COOMe)$_4$CH$_3$)] (7b)

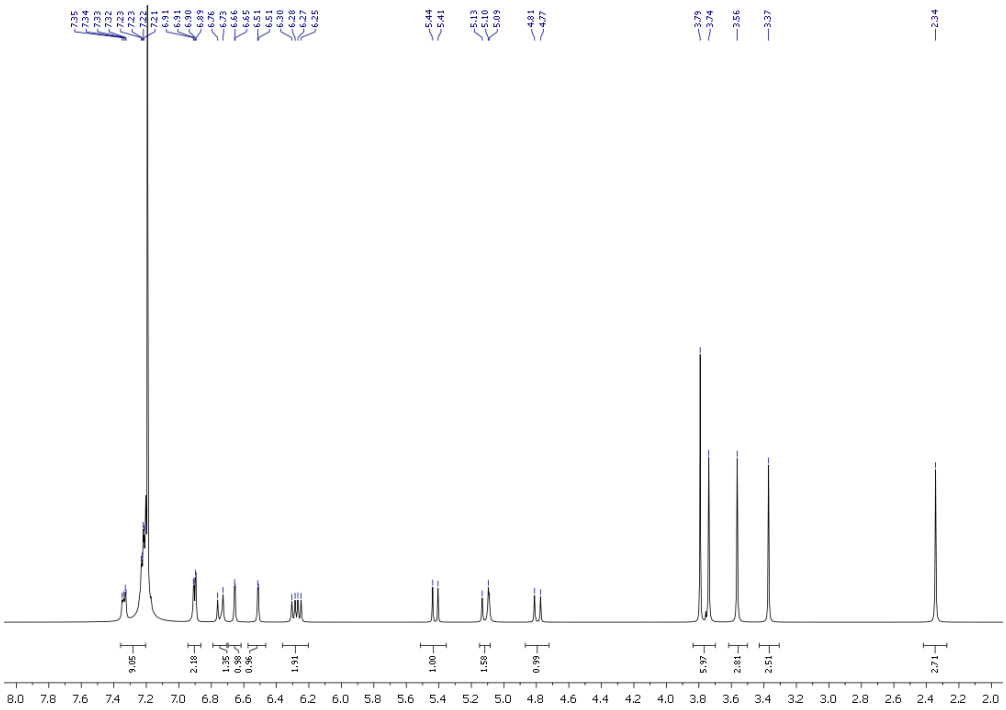

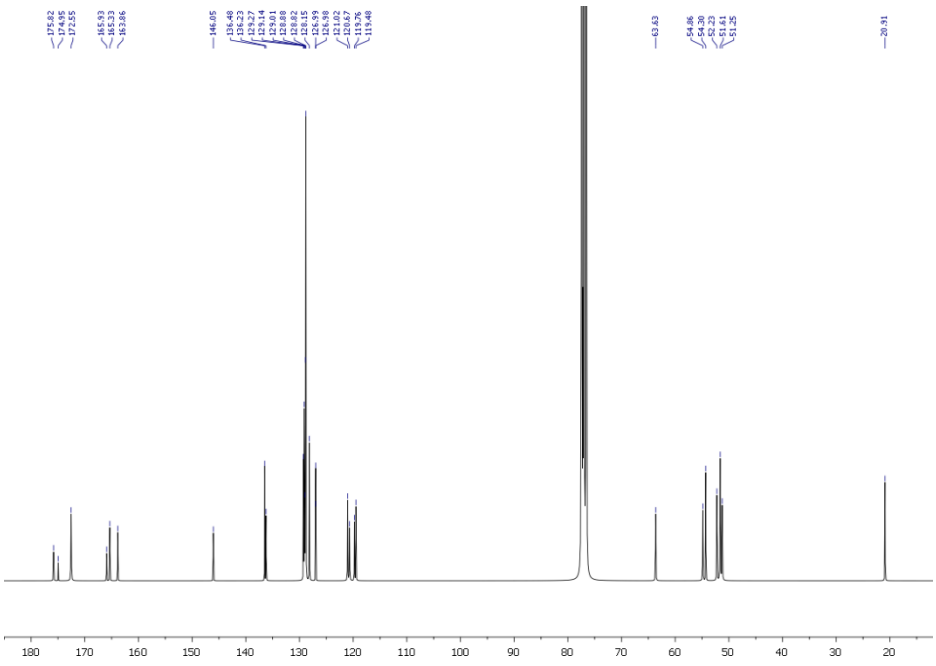

^{1}H NMR, ^{31}P{^{1}H} NMR and ^{13}C{^{1}H} NMR spectra of *trans*-[Pd(PPh$_3$)$_2$Cl(C$_2$(COOMe)$_2$CH$_3$)] (8a)

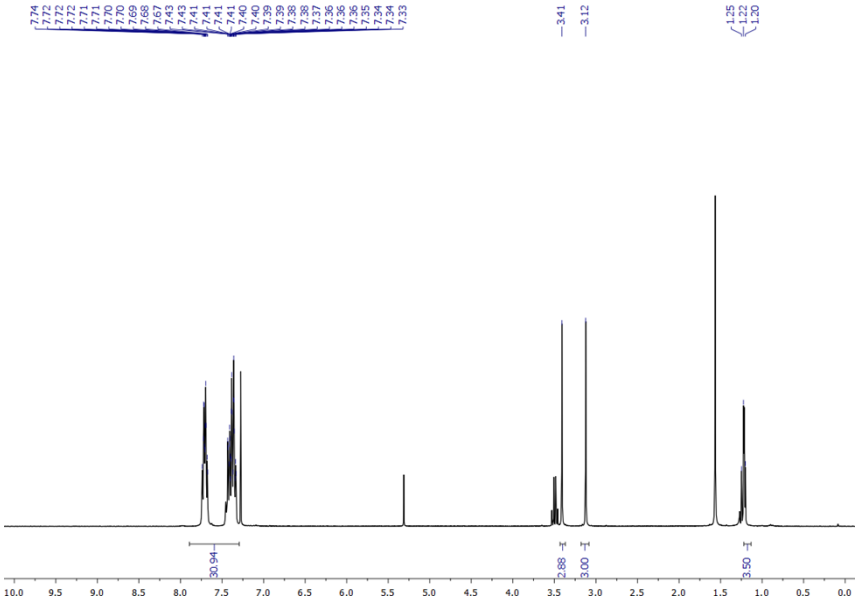

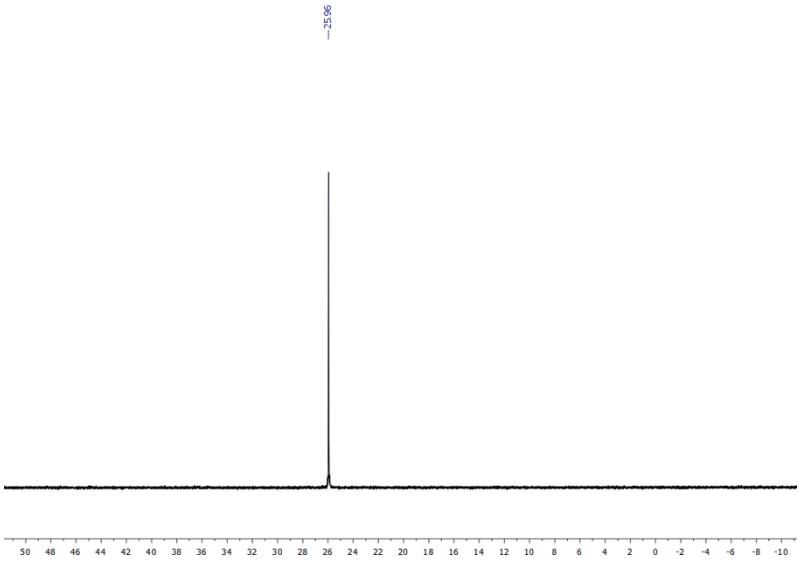

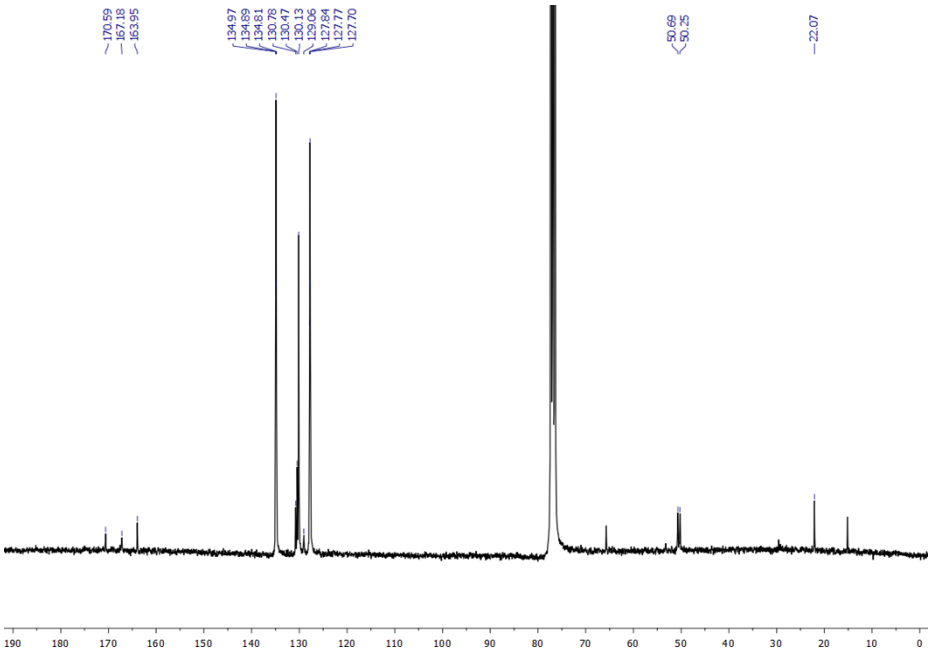
170.59
167.18
163.95
134.97
134.89
134.81
130.78
130.47
130.13
129.06
127.84
127.77
127.70
50.69
50.25
22.07
190
180
170
160
150
140
130
120
110
100
90
80
70
60
50
40
30
20
10
0

^{1}H NMR, ^{31}P{^{1}H} NMR and ^{13}C{^{1}H} NMR spectra of *trans*-[Pd(PPh$_3$)$_2$Cl(C$_4$(COOMe)$_4$CH$_3$)] (8b)

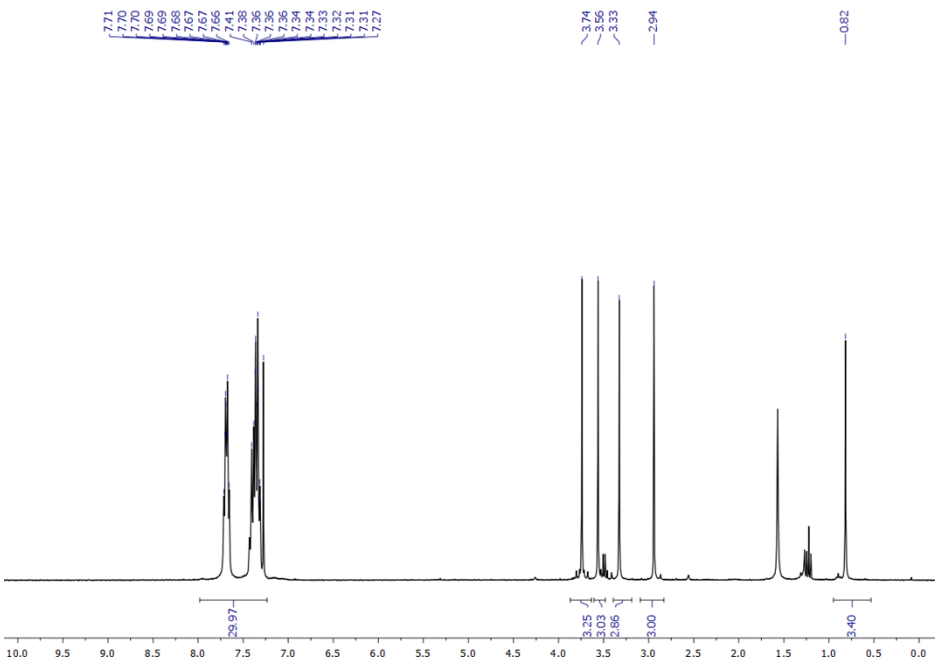

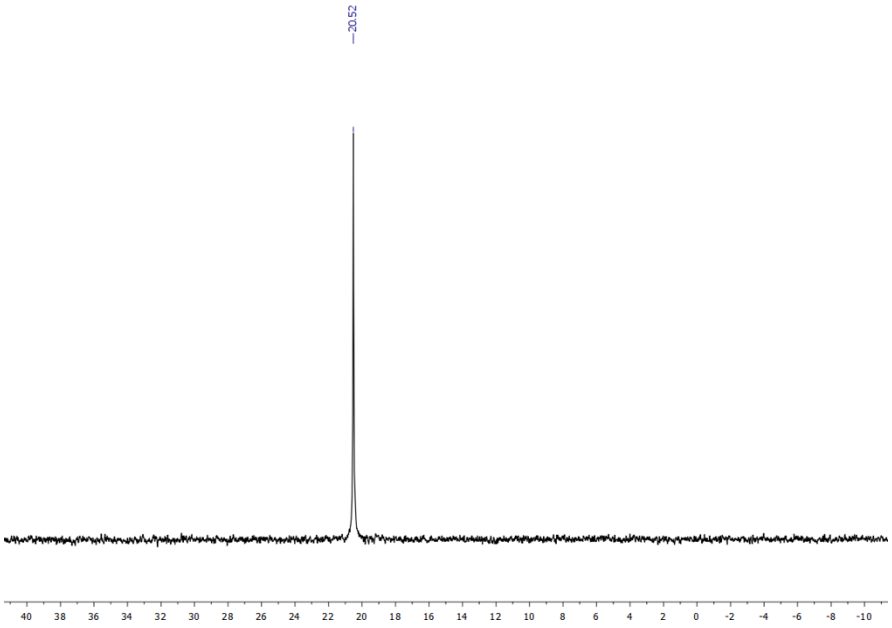

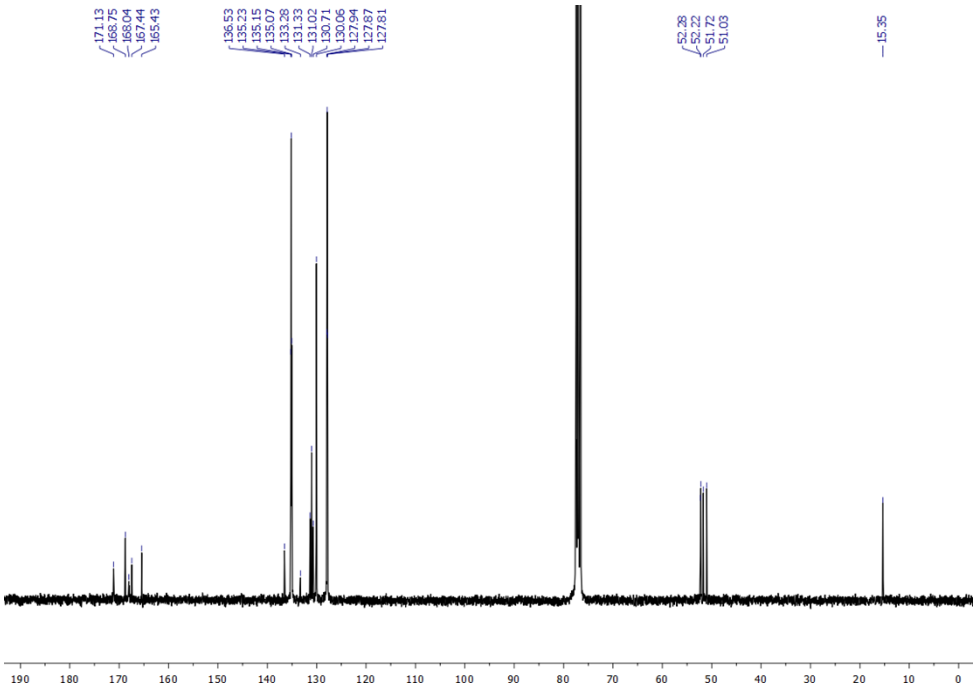
171.13
168.75
168.04
167.44
165.43
136.53
135.23
135.15
135.07
133.28
131.33
131.02
130.71
130.06
127.94
127.87
127.81
52.28
52.22
51.72
51.03
15.35
190
180
170
160
150
140
130
120
110
100
90
80
70
60
50
40
30
20
10
0

^{1}H NMR, ^{31}P{^{1}H} NMR and ^{13}C{^{1}H} NMR spectra of *trans*-[Pd(PTA)$_2$Cl(C$_2$(COOMe)$_2$CH$_3$)] (9a)

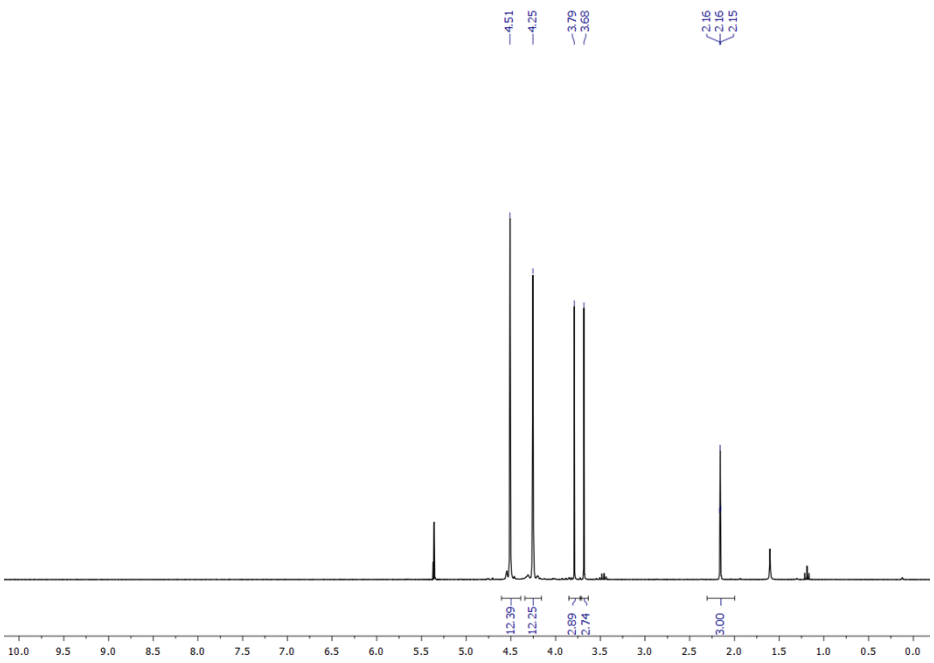

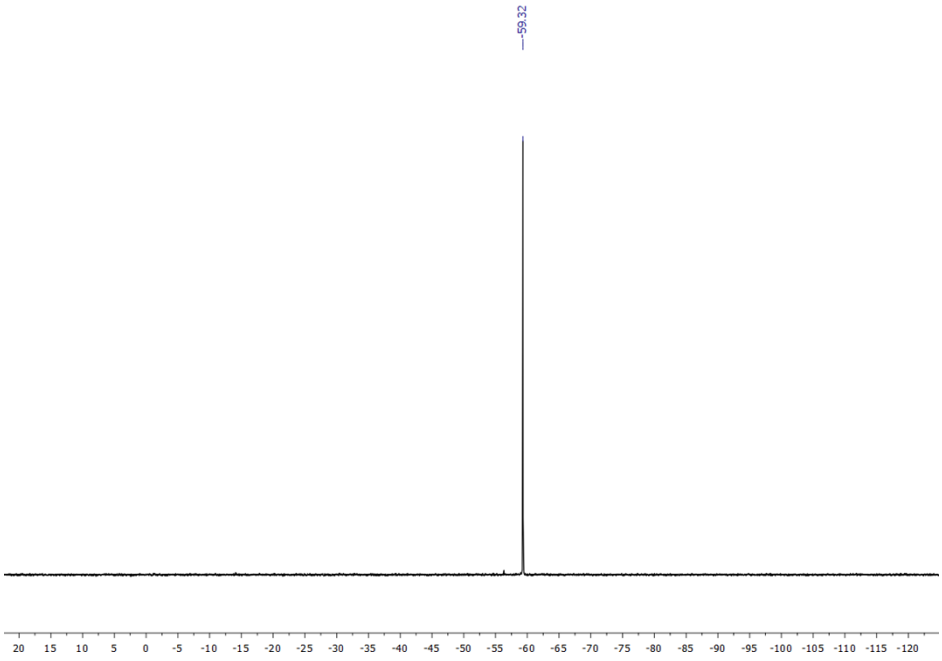

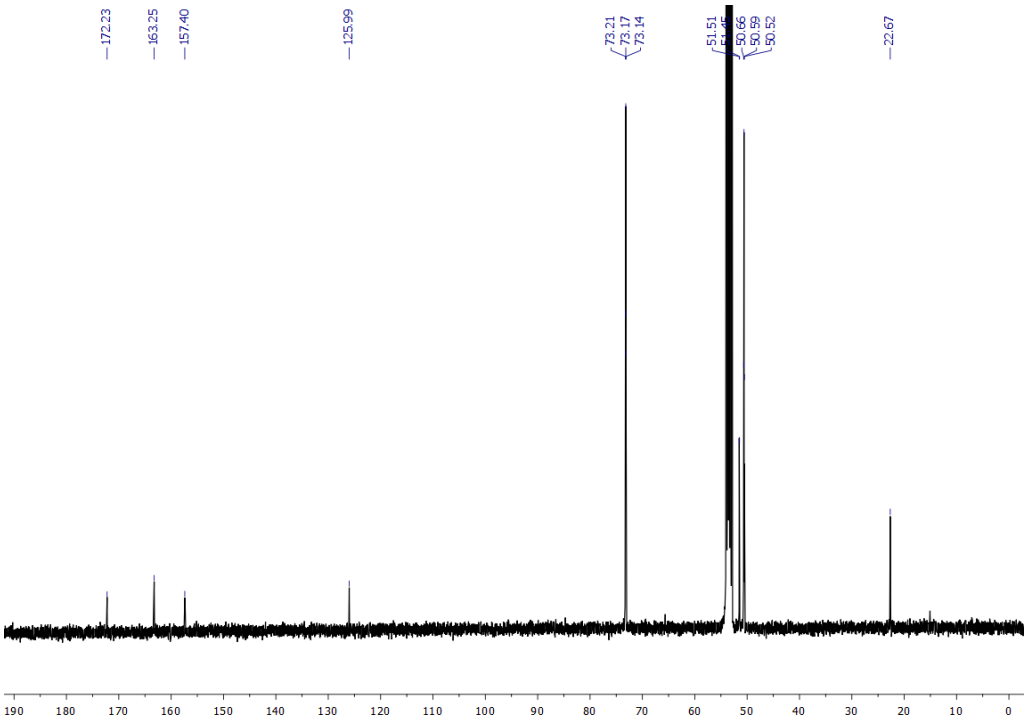
172.23
163.25
157.40
125.99
73.21
73.17
73.14
51.51
50.66
50.59
50.52
22.67
190
180
170
160
150
140
130
120
110
100
90
80
70
60
50
40
30
20
10
0

^{1}H NMR, ^{31}P{^{1}H} NMR and ^{13}C{^{1}H} NMR spectra of *trans*-[Pd(PTA)$_2$Cl(C$_4$(COOMe)$_4$CH$_3$)] (9b)

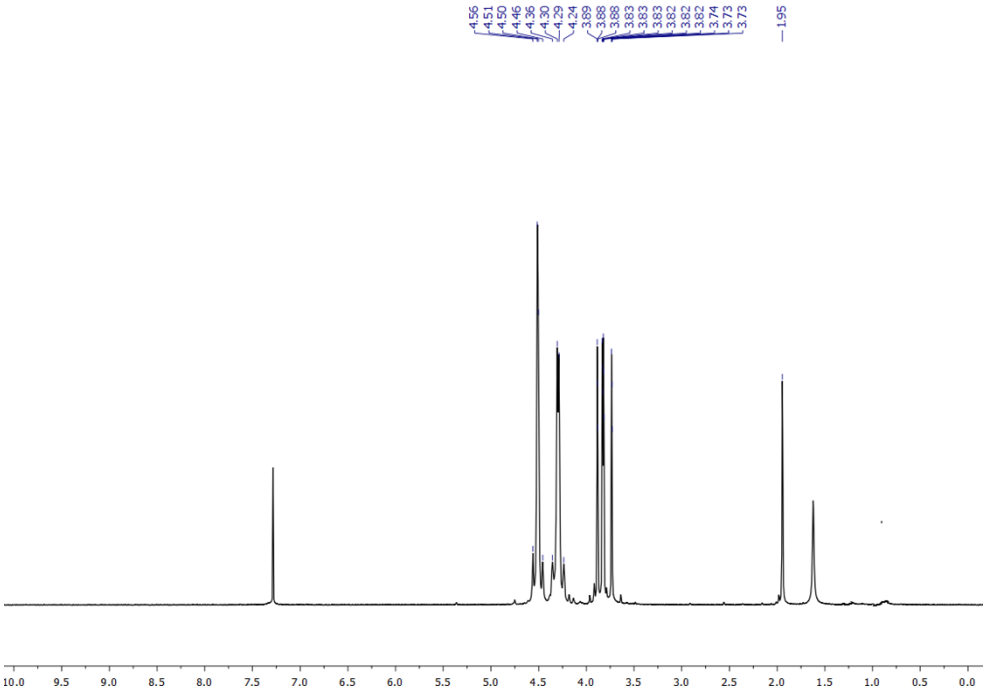

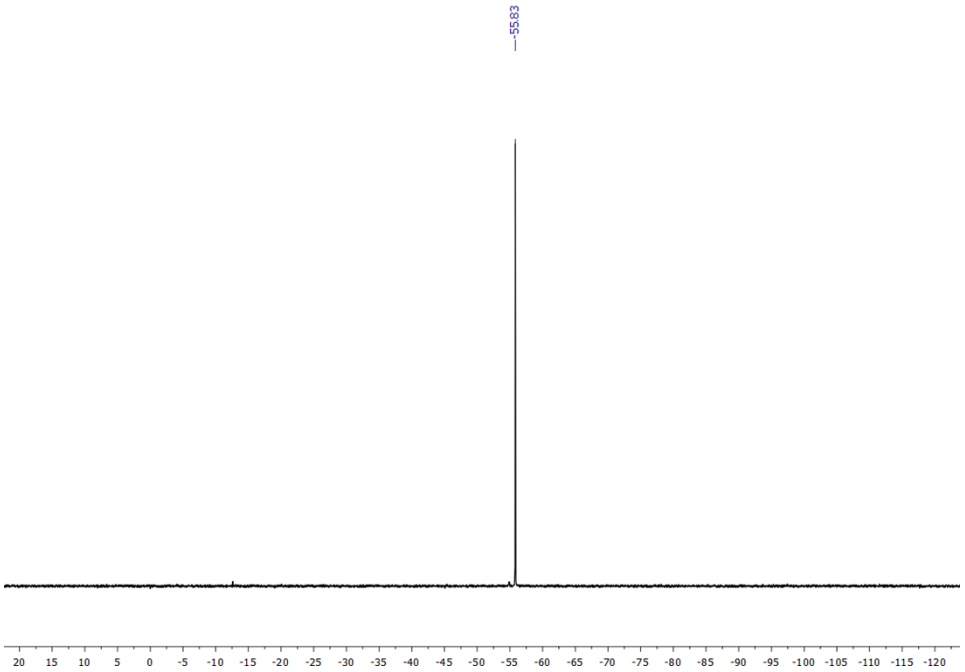

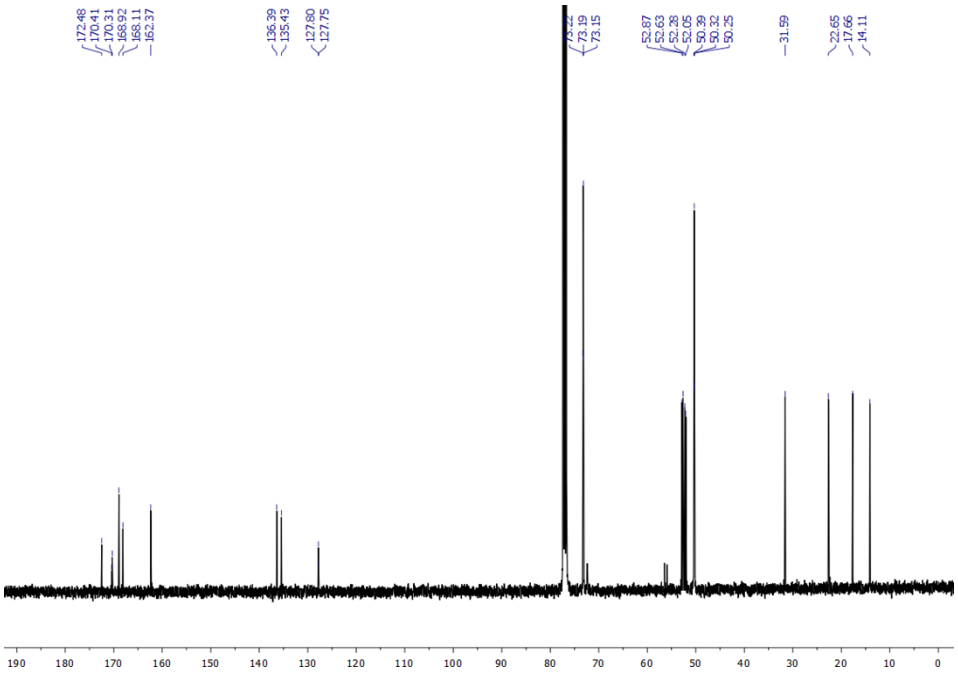
172.48
170.41
170.31
168.92
168.11
162.37
136.39
135.43
127.80
127.75
73.19
73.15
52.87
52.63
52.28
52.05
50.39
50.32
50.25
31.59
22.65
17.66
14.11
190
180
170
160
150
140
130
120
110
100
90
80
70
60
50
40
30
20
10
0

^{1}H NMR, ^{13}C{^{1}H} NMR spectra of *trans*-[Pd(AsPh$_3$)$_2$Cl(C$_2$(COOMe)$_2$CH$_3$)] (10a)

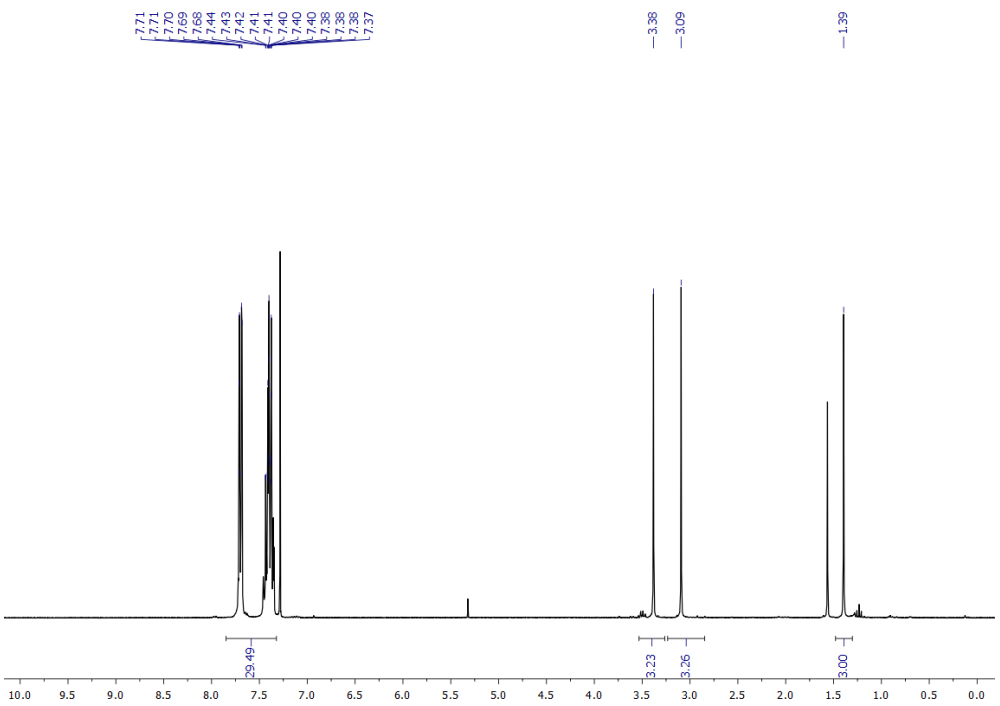

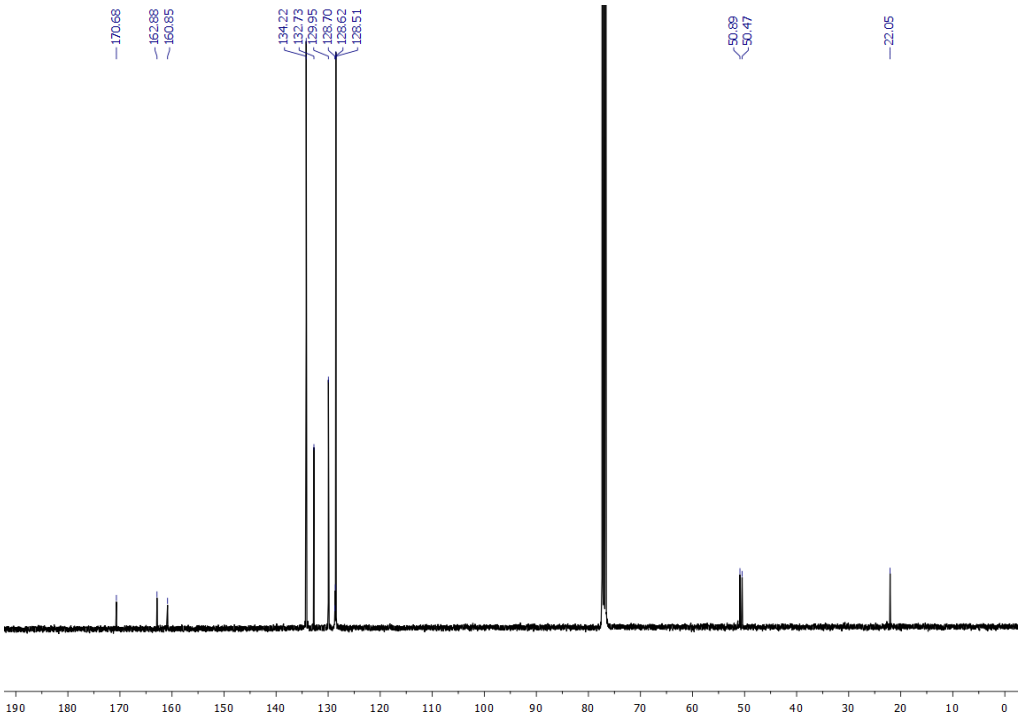

^{1}H NMR, $^{13}C\{^{1}H\}$ NMR spectra of *trans*-$[Pd(AsPh_3)_2Cl(C_4(COOMe)_4CH_3)]$ (10b)

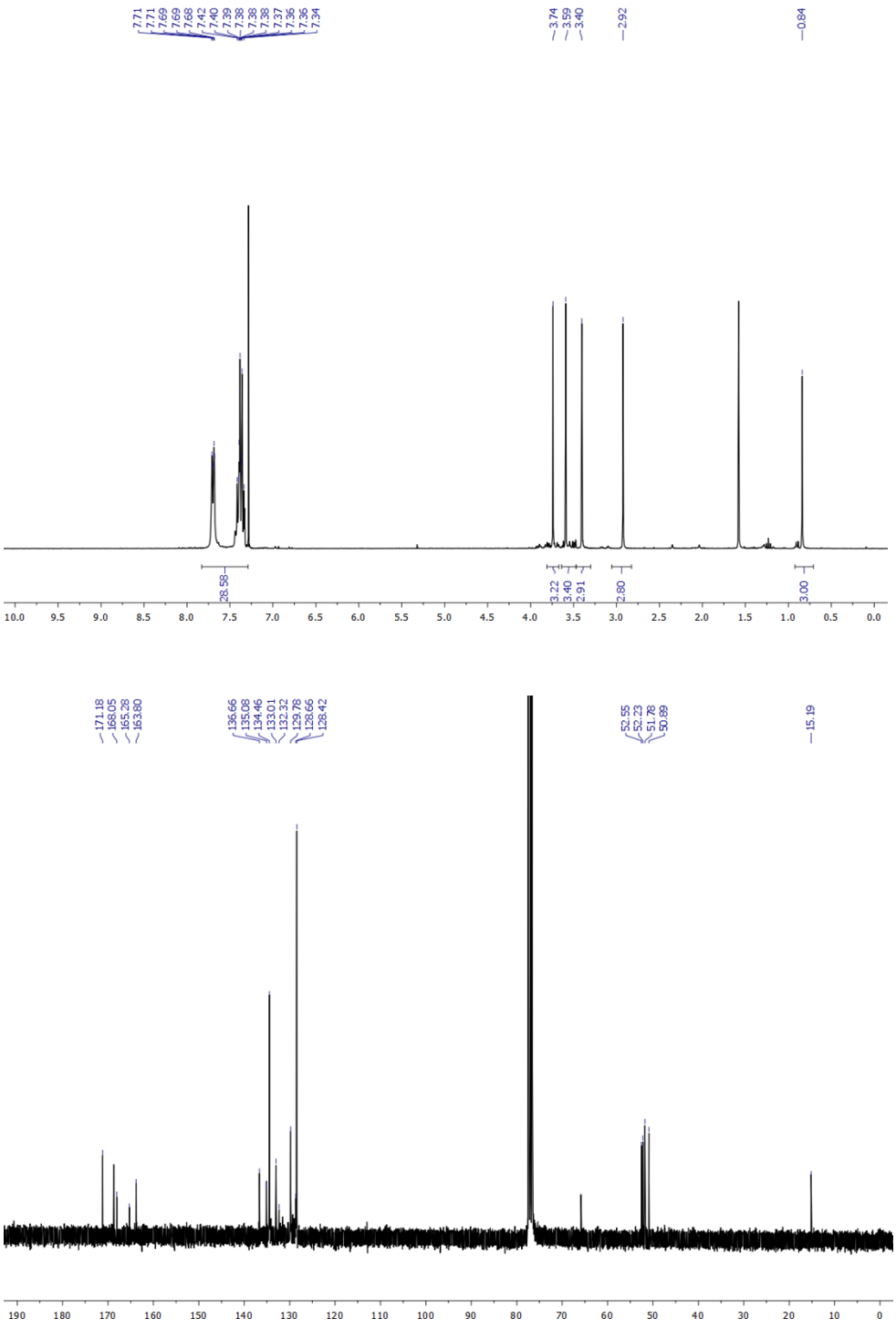

^{1}H NMR, $^{31}P\{^{1}H\}$ NMR and $^{13}C\{^{1}H\}$ NMR spectra of *trans*-[Pd(PTA)$_2$(C≡C-Ph)(C$_2$(COOMe)$_2$CH$_3$)] (13)

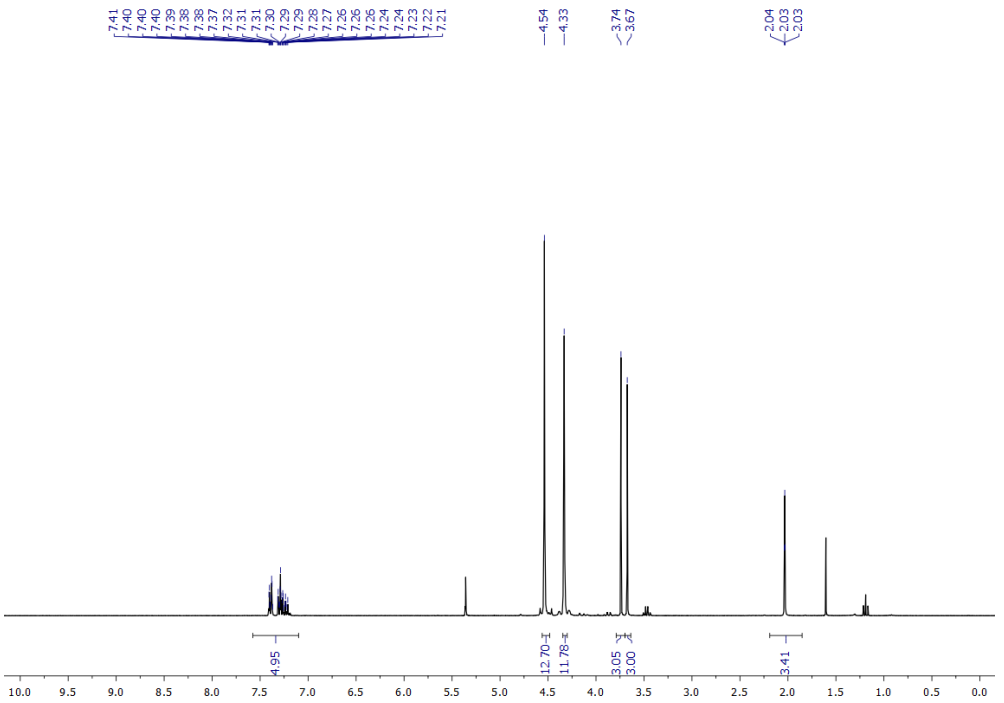

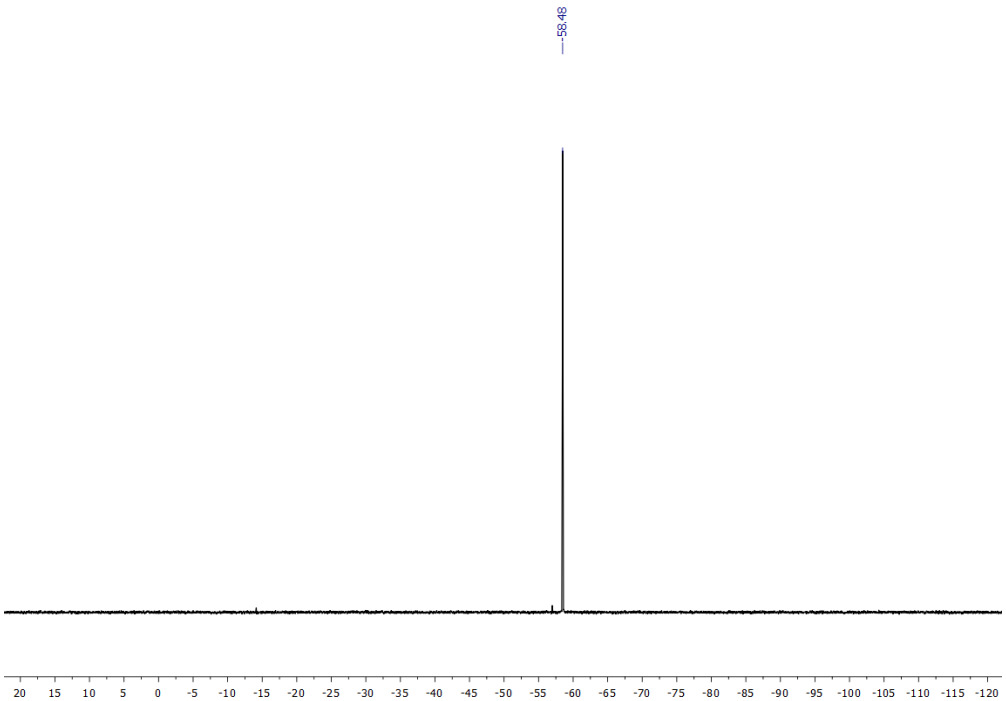

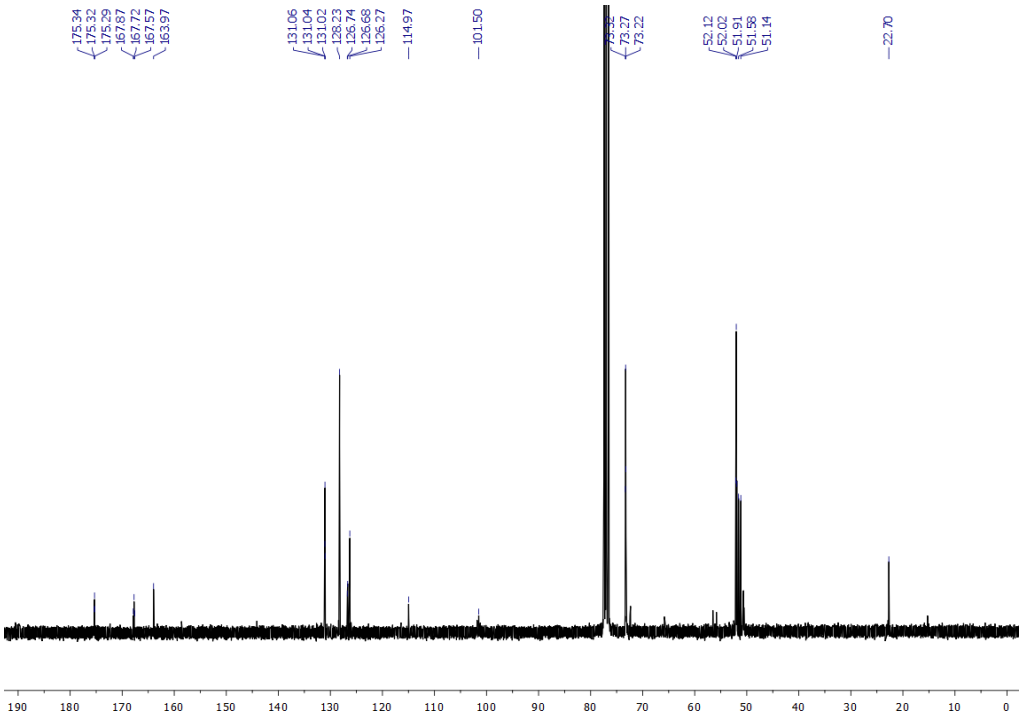
175.34
175.32
175.29
167.87
167.72
167.57
163.97
131.06
131.04
131.02
128.23
126.74
126.68
126.27
114.97
101.50
73.32
73.27
73.22
52.12
52.02
51.91
51.88
51.14
22.70
190
180
170
160
150
140
130
120
110
100
90
80
70
60
50
40
30
20
10
0

Crystallographic data

Table S2. Crystallographic data.

Compound	**2a**	**2b**	**3b**	**13**	**5a**
Formula	$[PdC_{19}H_{17}ClN_2O_4]\cdot CHCl_3$	$[PdC_{25}H_{23}ClN_2O_8]$	$[PdC_{27}H_{27}ClN_2O_8]$	$[PdC_{27}H_{38}N_6O_4P_2]\cdot CHCl_3$	$[PdC_{33}H_{34}ClO_4P_2]\ CHCl_3$
M/g·mol^{-1}	598.56	621.30	649.35	798.34	816.75
Space group	*1* *P* -1	*2* *P* -1	*3* *P* -1	*4* *P* -1	*5* *P* $na2_1$
Crystal system	Triclinic	Triclinic	Triclinic	Triclinic	Orthorhombic
a/Å	8.559(2)	8.605(2)	10.366(2)	10.743(2)	18.056(4)
b/Å	9.997(2)	8.866(2)	11.949(2)	12.747(3)	20.810(4)
c/Å	14.569(3)	17.383(3)	12.605(3)	13.560(3)	9.539(2)
α/°	104.46(3)	76.16(3)	82.50(3)	80.40(3)	90
β/°	90.63(3)	83.51(3)	68.40(3)	66.95(3)	90
γ/°	113.81(3)	77.13(3)	67.68(3)	86.12(3)	90
V/Å^3	1095.6(5)	1252.9(5)	1342.8(6)	1684.8(7)	3584.2(12)

6	*Z*	2	2	2	2	4
T/K		100(2)	100(2)	100(2)	100(2)	100(2)
D_c/g·cm^{-3}		1.814	1.647	1.606	1.574	1.514
F(000)		596	628	660	816	1656
μ/mm^{-1}		0.927	0.617	0.579	0.631	0.639
Measured Reflections		58846	89496	63021	79737	44667
Unique Reflections		11201	10923	11655	14689	15398
R_{int}		0.0463	0.0384	0.0380	0.0420	0.0441
Obs. Refl.ns [I≥2σ(I)]		10850	10662	11366	12953	15089
θ_{min}- θ_{max}/°		1.27 – 32.29	1.05 – 31.10	1.52 – 31.09	1.41 – 31.11	1.30 – 31.07
hkl ranges		-14,14; -16,14; -24,24	-14,14; -14,14; -28,28	-16,17; -18,18; -20,20	-17,17; -21,21; -22,22	-30,28; -32,31; -15,15
R(F^2) (Obs.Refl.ns)		0.0303	0.0321	0.0320	0.0417	0.0298
wR(F^2) (All Refl.ns)		0.0775	0.0853	0.0834	0.1156	0.0802
No. Variables		283	339	360	405	410
Goodness of fit		1.029	1.065	1.050	1.084	1.026
$\Delta\rho_{max}$; $\Delta\rho_{min}$/e·Å^{-3}		1.61; -2.21	1.04; -1.36	1.27; -1.62	1.29; -2.25	1.10; -0.74
CCDC Deposition N.		2343666	2343667	2343668	2343669	2343670

Table S3. Selected palladium coordination sphere distances and angles (Å and degrees) for **2a**.

2a (100 K) – $[PdC_{19}H_{17}ClN_2O_4]$

Distances		Angles	(°)
	6.1.1 (Å)		
Pd_1-C4_2	1.992(1)	C4_2-Pd_1-Cl_4	89.58(4)
Pd_1-N1_3	2.052(1)	C4_2-Pd_1-N1_3	95.74(5)
Pd_1- N10_3	2.098(1)	N1_3-Pd_1-N10_3	80.52(5)
Pd_1-Cl_4	2.286(1)	N10_3-Pd_1-Cl_4	94.18(4)

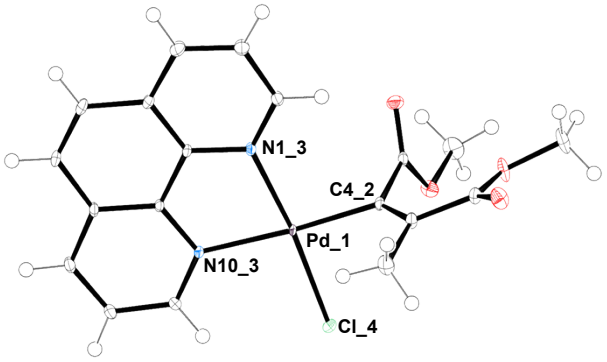

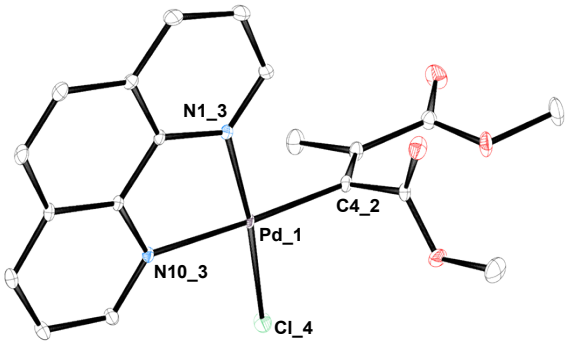

Table S4. Selected palladium coordination sphere distances and angles (Å and degrees) for **2b**.

2b (100 K) - $[PdC_{25}H_{23}ClN_2O_8]$

Distances		Angles	(°)
	6.1.2 (Å)		
Pd_1-C4_2	1.989(1)	C4_2-Pd_1-Cl_4	91.62(5)
Pd_1-N1_3	2.042(1)	C4_2-Pd_1-N1_3	93.21(5)
Pd_1- N10_3	2.106(1)	N1_3-Pd_1-N10_3	80.75(5)
Pd_1-Cl_4	2.291(1)	N10_3-Pd_1-Cl_4	94.43(4)

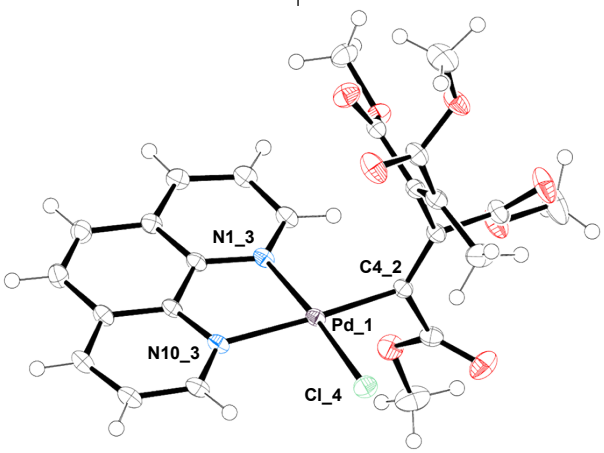

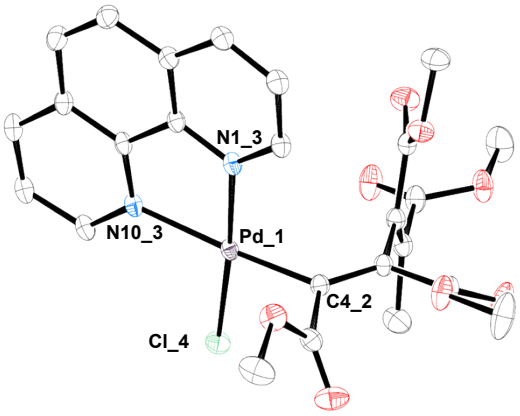
N1_3
N10_3
Pd_1
C4_2
Cl_4

Table S5. Selected palladium coordination sphere distances and angles (Å and degrees) for **3b**.

3b (100 K) - $[PdC_{27}H_{27}ClN_2O_8]$

Distances		**Angles**	**(°)**
	6.1.3 (Å)		
Pd_1-C4_2	1.989(1)	C4_2-Pd_1-Cl_4	84.44(5)
Pd_1-N1_3	2.058(1)	C4_2-Pd_1-N1_3	96.32(6)
Pd_1- N10_3	2.156(1)	N1_3-Pd_1-N10_3	79.42(5)
Pd_1-Cl_4	2.310(1)	N10_3-Pd_1-Cl_4	99.35(5)

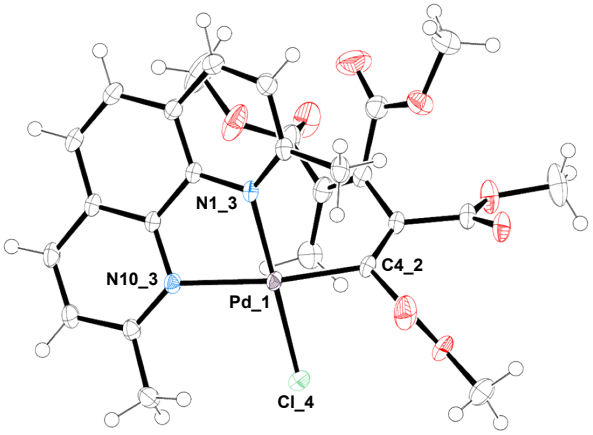

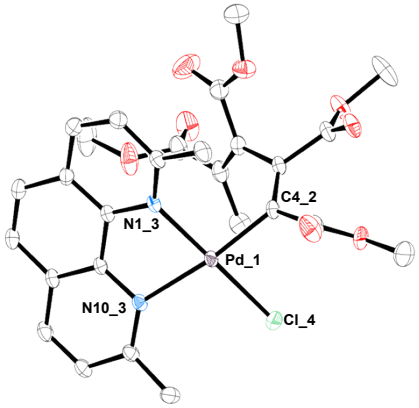

Table S6. Selected palladium coordination sphere distances and angles (Å and degrees) for **13**.

13 (100 K) - $[PdC_{27}H_{38}N_6O_4P_2]$

Distances		**Angles**	(°)
	6.1.4 (Å)		
Pd_1-C4_2	2.062(2)	C4_2-Pd_1-P1_3	92.51(5)
Pd_1-P1_3	2.289(1)	P1_3-Pd_1-C_5	90.53(5)
Pd_1- P1_4	2.276(1)	P1_4-Pd_1-C_5	87.63(5)
Pd_1-C_5	2.043(2)	P1_4-Pd_1-C4_2	89.39(5)

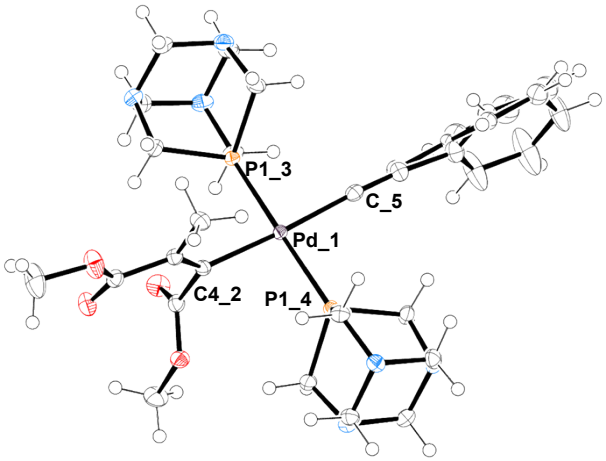

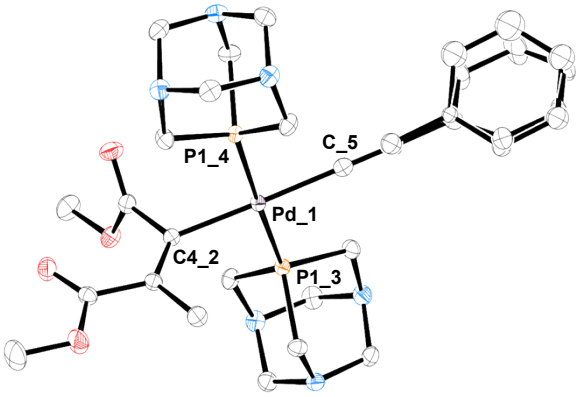

Table S7. Selected palladium coordination spheres distances and angles (Å and degrees) for **5a**.

5a (100 K) – $[PdC_{33}H_{34}ClO_4P_2]$

Distances		**Angles**	(°)
	6.1.5 (Å)		
Pd_1-C4_2	2.059(2)	C4_2-Pd_1-P1_3	92.78(6)
Pd_1-P1_3	2.233(1)	P1_3-Pd_1-P2_3	85.36(2)
Pd_1- P2_3	2.304(1)	P2_3-Pd_1-Cl_4	93.32(2)
Pd_1-Cl_4	2.366(1)	Cl_4-Pd_1-C4_2	88.55(6)

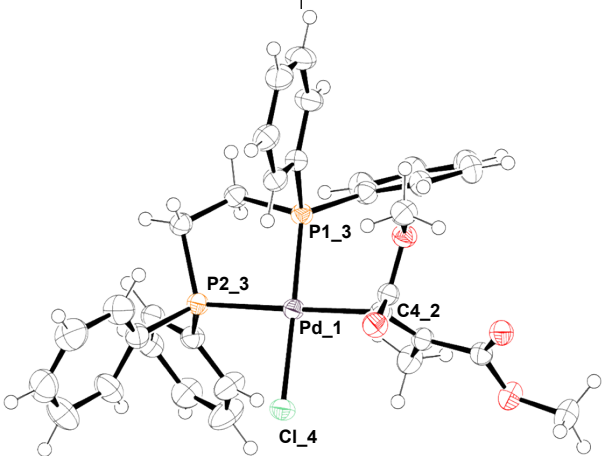

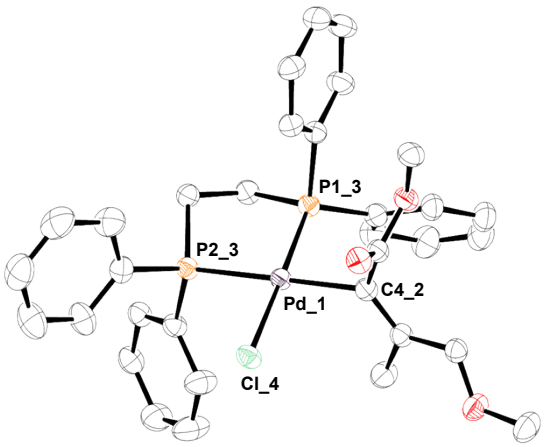

References

[1] L. Canovese, F. Visentin, G. Chessa, P. Uguagliati, C. Santo, A. Dolmella, *Organometallics,* 2005, **24**, 3297–3308.

[2] T. Scattolin, L. Canovese, F. Visentin, C. Santo, N. Demitri, *Polyhedron,* **2018**, **154**, 382–389

[3] T. Scattolin, E. Bortolamiol, I. Caligiuri, F. Rizzolio, N. Demitri, F. Visentin, *Polyhedron,* 2020, **186**, 114607

[4] O. Kopper, C. J. De Witte, K. Lõhmussaar, J. E. Valle-Inclán, N. Hami, L. Kester, A. V. Balgobind, J. Korving, N. Proost, H. Begthel, L. M. Van Wijk, S. A. Revilla, R. Theeuwsen, M. Van De Ven, M. J. Van Roosmalen, B. Ponsioen, V. W. Ho, B. G. Neel, T. Bosse, K. N. Gaarenstroom, H. Vrieling, M. P. G. Vreeswijk, P. J. Van Diest, P. O. Witteveen, T. N. Jonges, J. L. Bos, A. Van Oudenaarden, R. P. Zweemer, H. J. G. Snippert, W. P. Kloosterman, H. Clevers, *Nat. Med.,* 2019, **25**, 838–849.

[5] A. Lausi, M. Polentarutti, S. Onesti, J. R. Plaisier, E. Busetto, G. Bais, L. Barba, A. Cassetta, G. Campi, D. Lamba, A. Pifferi, S. C. Mande, D. D. Sarma, S. M. Sharma, G. Paolucci, *Eur. Phys. J. Plus,* 2015, **130**, 43.

[6] W. Kabsch, *Acta Crystallogr. D Biol. Crystallogr.,* 2010, **66**, 125–132.

[7] P. R. Evans, G. N. Murshudov, *Acta Crystallogr. D Biol. Crystallogr.,* 2013, **69**, 1204–1214.

[8] G.M. Sheldrick, *Acta Crystallogr. A*, 2015, **71**, 3.

[9] G.M. Sheldrick, *Acta Crystallogr. C*, 2015, **71**, 3.

[10] P. Emsley, B. Lohkamp, W. G. Scott, K. Cowtan, *Acta Crystallogr. D Biol. Crystallogr.,* 2010, **66**, 486–501.

[11] L. J. Farrugia, *J. Appl. Crystallogr.,* 2012, **45**, 849–854.

[12] L. Schrodinger, The PyMOL Molecular Graphics System. Schrodinger, 2015**,** LLC. http://www.pymol.org.